

## Article

# Geological Characteristics and Paleoenvironmental Evolution of Fine-Grained Sediments in the Third Member of the Xujiahe Formation in the Western Sichuan Depression, SW China

Yunfei Lu <sup>1,2</sup>, Jingchun Tian <sup>1,2,\*</sup>, Qingshao Liang <sup>1,2</sup> and Xiaobing Lin <sup>1,2</sup><sup>1</sup> Institute of Sedimentary Geology, Chengdu University of Technology, Chengdu 610059, China<sup>2</sup> State Key Laboratory of Oil & Gas Reservoir Geology and Exploitation, Chengdu University of Technology, Chengdu 610059, China

\* Correspondence: tj@cdut.edu.cn

**Abstract:** This study investigated, in detail, the characteristics of the Late Triassic fine-grained sediments in the third member of the Xujiahe Formation (Xu-3 Member), in the Western Sichuan Depression, and the paleoenvironmental evolution during their deposition through petrological interpretation, mineralogical composition characterization, and element geochemical analysis. According to the mineralogical composition, the Xu-3 Member can be divided into two petrological types, namely clayey fine-grained felsic sedimentary rocks and lime fine-grained felsic sedimentary rocks. The main mineral components are siliceous, clay, and carbonate minerals. Through the cluster analysis of major elements, all samples could be divided into two types with different major elemental characteristics. Trace elements exhibited distinct Sr depletion, relative enrichment of large ion lithophile elements, and high field strength elements. Two REE enrichment patterns were observed, which could be attributed to differences in the provenance area and tectonic background. The paleoclimate of the sedimentary area was warm and humid, but it was hotter and drier in the southern and central parts of the depression. The change trend of paleo-productivity was consistent with the paleoclimate. The waters in the sedimentary environment were mainly brackish water to saline water, with fresh water in the southern part of the depression. The paleo-redox conditions of the waters were mainly sub-oxidation to sub-reduction, but the southern part of the depression was more oxidative. The provenance area experienced a moderate degree of chemical weathering under a warm and humid paleoclimate, same as the depositional area. However, the depositional environments differed between the northern and south-central parts of the depression.

**Keywords:** geological characteristics; paleoenvironment; fine-grained sediments; Xu-3 member

**Citation:** Lu, Y.; Tian, J.; Liang, Q.; Lin, X. Geological Characteristics and Paleoenvironmental Evolution of Fine-Grained Sediments in the Third Member of the Xujiahe Formation in the Western Sichuan Depression, SW China. *Minerals* **2023**, *13*, 510. <https://doi.org/10.3390/min13040510>

Academic Editors: Roberto Buccione and Rabah Kechiched

Received: 11 February 2023

Revised: 30 March 2023

Accepted: 1 April 2023

Published: 2 April 2023



**Copyright:** © 2023 by the authors. Licensee MDPI, Basel, Switzerland. This article is an open access article distributed under the terms and conditions of the Creative Commons Attribution (CC BY) license (<https://creativecommons.org/licenses/by/4.0/>).

## 1. Introduction

Fine-grained sediments are of high significance in the reconstruction of the Earth's environments because they can continuously record the sedimentary history of their depositional environment [1,2]. They primarily form in the deep-water areas of oceans and lakes, and consist of clay-grade and chalk-grade clastic particles of less than 62.5 µm in size [3,4]. Fine-grained sedimentary rocks are those containing more than 50% of fine-grained sediments, and they account for approximately 70% of global sedimentary rocks [5,6]. In particular, organic-rich black shale is not only the main source rock of oil and gas, but also an important unconventional oil and gas reservoir [5,7]. In recent decades, geochemical methods using major, trace, and rare earth elements (REEs) in fine-grained sediments have been used to establish the sedimentary environment and characteristics of the provenance [8–11].

The West Sichuan Depression is located in front of the Longmenshan Nappe structural zone in the northwestern part of the Sichuan Basin, and it is a foreland basin that has formed in the western part of the Sichuan Basin since the Late Triassic due to the recoil

of the Longmenshan Mountains, which has undergone several tectonic movements in the Indo-Chinese, Yanshan, and Himalaya regions [12].

The Xujiache Formation, as a set of high-quality continental reservoirs widely distributed in the Sichuan Basin, has been the focus of research for a long time [13–15]. The Xujiache Formation of the Upper Triassic is also the main production layer in the middle section of the Western Sichuan Depression [16]. The first, third, and fifth members of the Xujiache Formation mainly develop argillaceous deposits and coal seams, which are good hydrocarbon source rocks. The second and fourth members of the Xujiache Formation mainly develop sandstone deposits, which are the main reservoir sections. Oil and gas exploration have achieved great success [17]. Previous studies mainly focused on sandstone reservoirs in the Xujiache Formation [18–20]. The research achievements of predecessors on fine-grained sediments of the Xujiache Formation in the Sichuan Basin were mainly on the organic geochemical characteristics and reservoir performance of hydrocarbon source rocks [13,21,22]. Regarding the fine-grained sediments of the Xujiache Formation in the Western Sichuan Depression, the research focus has also been on the organic geochemical characteristics of tight reservoirs and source rocks, such as the identification of tight reservoirs and diagenetic logging facies [23,24], as well as the organic geochemical characteristics, hydrocarbon generation potential, redox conditions, and “sweet spot” reservoir distribution [25,26]. In contrast, the tectonic setting and provenance of the fine-grained sediments of the Xujiache Formation in the Western Sichuan Depression have rarely been investigated [16,27]. Furthermore, only a few studies have investigated the third member of the Xujiache Formation (Xu-3 Member) in the Western Sichuan Depression, especially its paleoenvironment.

This study investigated the mineralogical, petrological, and geochemical characteristics of fine-grained sediments of the Xu-3 Member, analyzed the evolution characteristics of the paleoenvironment, and deduced the coupling relationship between the chemical weathering degree of the provenance area and the paleoenvironment of the sedimentary area using various basic geological methods and geochemical analysis methods. To this end, fine-grained sediments of the Xu-3 Member were sampled from the Jinhe (JH) section and Tiangongmiao (TGM) section in the Western Sichuan Depression, and some previous research data on the Jinhe (CJH) and Longcanggou (LCG) sections were collected. The findings provide deeper insight into the evolution of the Western Sichuan Depression during the sedimentation period of the Xu-3 Member, and reveal the dominant factors controlling paleoenvironment evolution in a continental lacustrine sediment, which could serve as a guide for shale gas exploration.

## 2. Geological Setting

The Western Sichuan Depression is located in South China (Figure 1a), at the west of the Sichuan Basin, the eastern margin of the Qinghai-Tibet Plateau, and the western margin of the Yangtze Craton [28–31]. In the northwest of the depression, together with the Songpan-Ganzi fold belt and Longmenshan orogenic belt, it forms a plate boundary collision system [28,32,33]. It lies adjacent to the Qinling-Dabashan orogenic belt in the northeastern part, the North China Plate in the northern part, and the Central Sichuan paleo uplift in the southeastern part [30,34]. The Jiangnan-Xuefeng Mountain orogenic belt of the Yangtze Plate lies at the southeast edge of the depression, and the Emei-Washan paleo uplift of the Sanjiang orogenic belt and the KangDian paleocontinent lies at the southwestern margin (Figure 1b). The depression comprises typical continental lacustrine sediments of the Late Triassic [35].

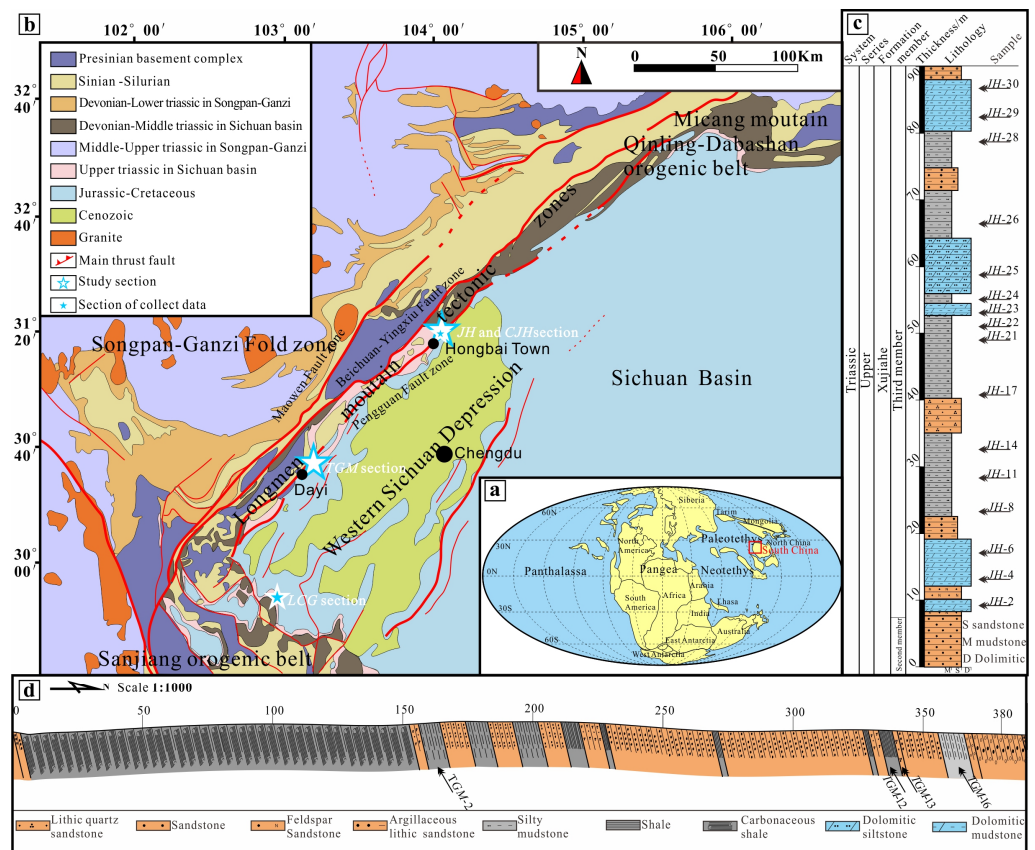


**Figure 1.** Geological sketch of the Western Sichuan Depression and histogram of the JH section and TGM section. (a) Paleogeographic Map of the Late Triassic (According to [36] revised); (b) Geological map of the Western Sichuan Depression (According to [31] revised); (c) JH section Histogram; (d) TGM section Histogram.

The Xujiahe Formation comprises a set of siliciclastic rocks that were deposited during the transition from a marine-continental depositional environment to a terrestrial depositional environment in the Late Triassic [29,36,37]. Based on lithology, the Xujiahe Formation can be subdivided into six members from the bottom to top, and the sixth member was eroded due to uplift during the Triassic and Jurassic [15,37]. The first member is mainly composed of marl, shale, and siltstone, which are carbonate gentle slope-idal flat deposits. The sedimentary environments of the first, third, and fifth members were relatively calm, and the sediments are dominated by fine-grained sediments, mainly including mudstone, shale, and siltstone, interbedded with thin sandstone layers and coal seams, which constitute the main regional hydrocarbon source rocks [20,37,38]. The second member is dominated by sandstone, with conglomerate or pebbly coarse sandstone at the bottom, and a set of shale is often sandwiched in the middle and upper part, which is mainly braided river delta deposit (Figure 2j). The fourth member is mainly thick-bedded sandstone, with conglomerate at the bottom, and mainly composed of fan delta and braided river delta deposits (Figure 2k–l) [31,37,39–41].

The Sichuan Basin has a rich and diverse floral composition of the Xujiahe Formation. Based on comprehensive consideration of the overall perspective of the flora, as well as the spatial and temporal distribution pattern of the representative taxonomic type, anthrosophies, in the Xu-3 Member, it can be concluded that the geological age of the Xu-3 Member is the Rhaetian [42]. The uppermost bed of the Xu-3 Member yields a relatively abundant and diverse fossil plant taxa. The dominant elements are represented by neo calamites, ferns, and cycads, and the diversity of the conifers is higher compared to that of other members [43,44]. The palynomorphs of the Xu-3 Member are well preserved

and are highly diverse, with 136 species of spores and pollen assigned to 63 genera [45]. The high diversity of conifers and the first appearance of ginkgoes in the Xu-3 Member demonstrate that the paleoclimate during the deposition was warm and humid [43–45].

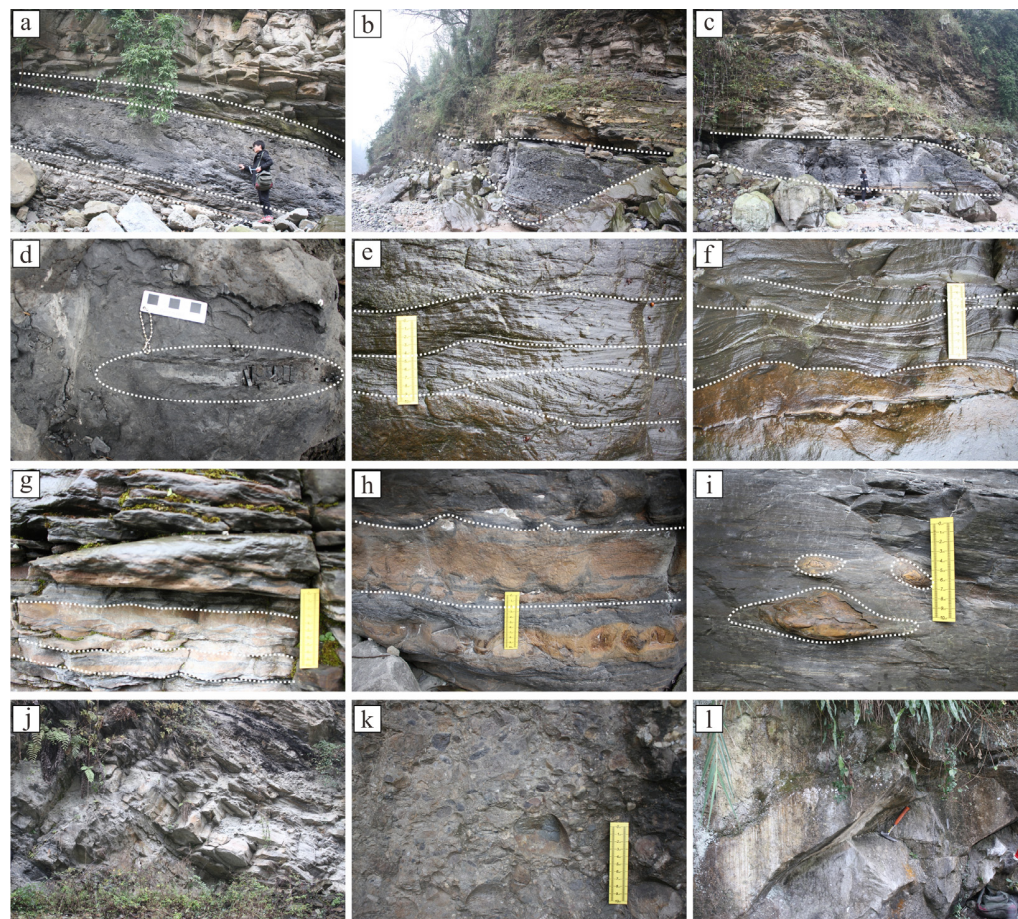


**Figure 2.** Field outcrop chart of fine-grained rocks of the Xu-3 Member in the Western Sichuan Depression. (a–c) Exposure of fine-grained sedimentary rocks of the Xu-3 Member in the JH section; (d) Fossil plant stems in the Xu-3 Member; (e,f) Trough cross bedding of the Xu-3 Member in the TGM section; (g) Flaser bedding in the Xu-3 Member; (h) Flame structure bedding; (i) Lenticular siderite nodule; (j) Sandstone of the Xu-2 Member in the TGM section; (k) Conglomerates at the boundary between the Xu-3 Member and the Xu-4 Member in the TGM section; (l) Sandstone of the Xu-4 Member in the TGM section.

The JH section is located near the Jinhe River, beside the road from Hongbai Town to Jinhe Village. The section is well exposed in the field and partially covered, with clear contact relationships. The exposed thickness of fine-grained sediments in the Xu-3 Member of the section is approximately 90 m (Figures 1c and 2a–i).

The TGM section is located near Tiangong Temple in Dayi Country, from which the Xujiage Formation can be observed along the road. The formation shows good continuity from the Xu-2 Member to the Xu-4 Member, and the Xu-3 Member is exposed for nearly 400 m. However, the fine-grained sediments are severely weathered, mostly covered by vegetation, and poorly exposed (Figures 1d and 2j–l).

### 3. Samples and Methods

In this study, a total of twenty fine-grained sediments samples were selected for research and analysis, of which sixteen samples were taken from the JH section (Figure 1b)

and four samples were taken from the TGM section (Figure 1c). All the samples were taken from fresh rocks without cracks in the inner layer of the outcrop to ensure purity.

Flakes identification was completed at the Institute of Sedimentary Geology, Chengdu University of Technology. Microscopic images were acquired using an optical microscope (Nikon E600 POL, made in Tokyo, Japan).

Scanning electron microscope (SEM) observations were completed at the Sinopec Zhongyuan Oilfield Geological Laboratory, using the Thermo Fisher Scientific Prisma E, SEM (Made in Waltham, MA, USA). Energy dispersive X-ray spectroscopy (EDAX) was also conducted, following the SY/T 5162-2014 standard. For the SEM observation, each sample was fixed on the sample table with conductive tape, the fixed sample was gilded, and the gilded sample was finally placed in the sample bin for observation.

A total of twenty samples were cleaned in an ultrasonic bath for 15 min to remove surface contamination, then washed with deionized water and air-dried at 50 °C until dry. All the samples were triturated to 200 mesh (75 µm) before analysis. These were crushed in an agate mortar and ground to a fine powder. These powder samples were used for whole rock X-ray diffraction (XRD), whole rock geochemical analysis, and total organic carbon (TOC) analysis.

Whole rock XRD analysis was completed at the Keyuan Engineering Technology Testing Center in Sichuan Province, using the X'pert Powder XRD system (Malvern Panalytical, Amsterdam, Netherlands), following the SY/T 5163-2018 standard. Sample preparation before testing included extracting clay minerals according to Stokes' rule. First, we removed the carbonate from the powder samples below 200 mesh, placed the powder sample in a beaker, slowly added dilute hydrochloric acid diluted to 5%, and continuously stirred with a glass rod until there were no bubbles. We tested the PH value of the solution at this time, and if it was less than 7, it indicated that the carbonate had reacted completely. Next, to remove organic matter, we centrifuged the carbonate-removed sample until the PH value was equal to 7, added 6% hydrogen peroxide, and stirred evenly. The reaction time generally exceeded 8 h. After that, we repeatedly washed the sample to make its pH value equal to 7 in order to make a suspension. The final natural sedimentation separation was less than 2 µm suspended particles, and was centrifuged to obtain a clay mineral sample.

Whole rock geochemical analysis was completed at the ALS Chemex (Guangzhou, China) Co., Ltd. During sample preparation, 300 g of broken samples were ground to 75 µm (200 meshes). During the test, the ambient temperature was 25 °C, and relative humidity was 50%. For the detection of major elements, the samples were dried at 105 °C, and the required weight was accurately weighed. Subsequently, the samples were placed in a platinum crucible, and a mixed flux of lithium tetraborate lithium metaborate lithium nitrate was added. After confirming complete and even mixing of the sample and flux, the mixture was melted at 1050 °C in a high-precision melting prototype, and the molten slurry was poured into the platinum mold, through which a sheet was formed. After cooling, the quality of the sheet was confirmed. In addition, the amounts of the main components were measured using the P61-XRF26s X-ray fluorescence (XRF) method. Regarding the precision and accuracy of the XRF spectroscopy, the relative deviation was controlled at (RD)% < 5(XRF), and the relative error was controlled at (RE)% < 5(XRF). During the detection of trace elements and REEs, the sample was added to the lithium metaborate/lithium tetraborate flux, mixed evenly, and melted in a furnace above 1025 °C. After cooling, the molten liquid was fixed to volume with nitric acid, hydrochloric acid, and hydrofluoric acid, and then analyzed using the M61-MS81 inductively coupled plasma mass spectrometry (ICP-MS) method. For the ICP-MS, RD, and RE were controlled at (RD)% < 10(XRF) and (RE)% < 10.

According to Chinese national standard GB/T 19145–2003, the content of TOC was determined using a LECO CS 230 carbon/sulfur analyzer at the Keyuan Engineering Technology Testing Center in Sichuan Province. Approximately 0.1 g of each powdered sample was analyzed for TOC. The samples were first reacted with 6 M HCL to remove carbonate. The residues were then rinsed at least six times until deemed neutral.

## 4. Results

### 4.1. Petrological and Mineralogical Characteristics

In the outcrop, the fine-grained sediments of the Xu-3 Member are mainly dark gray, with generally argillaceous texture (Figure 2a–c) and visible plant detritus fossils (Figure 2d). Sedimentary phenomena, including flaser bedding, trough cross bedding, and flame structure, are observable in the siltstone, indicating the possible occurrence of earthquakes and other events during deposition (Figure 2e–h). Thin layers of syngenetic siderite nodules can be observed in local intervals (Figure 2i), indicating that redox conditions are biased towards reduction [46]. According to the field lithological characteristics, fine-grained sediments of the Xu-3 Member can be divided into two types: mudstone and silty mudstone.

Polarizing microscope and SEM observations showed that the mudstone has argillaceous texture and felted structure (Figure 3a,b). The main type of clay mineral is illite, which is filiform under SEM (Figure 3g). Authigenic minerals, calcite, dolomite, and siderite were observed (Figure 3i,k). Organic matter and crust fossil detritus were also observed in individual samples (Figure 3b). A small number of silty laminae and argillaceous laminae could also be observed under the polarizing microscope (Figure 3d).

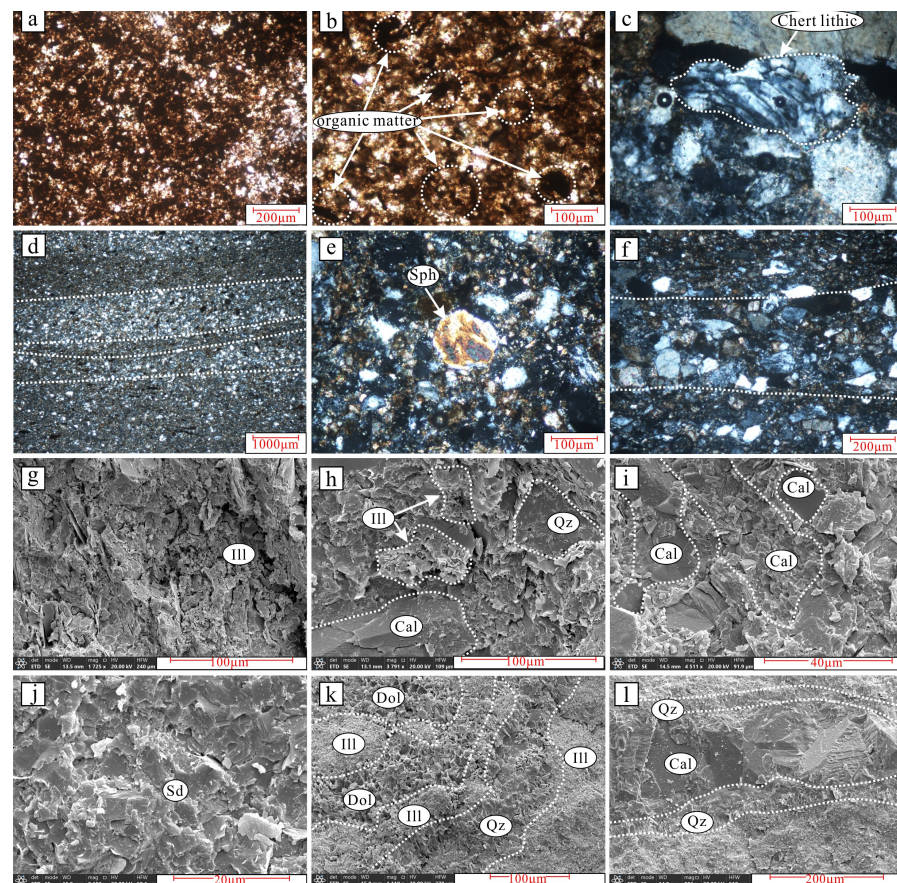


**Figure 3.** Micro characteristic chart of fine-grained sedimentary rock. Ill: Illite; Cal: Calcite; Sd: Siderite; Qz: Quartz; Dol: Dolomite; Sph: Sphere. (a) JH-30, muddy; (b) JH-20, argillaceous and organic matter; (c) JH-7, flint flake; (d) JH-5, silty grain layer; (e) JH-3, sphenes; (f) JH-3, sphenes; (g) JH-2, illite clay mineral; (h) JH-4, calcite crystals and lamellar illite filled intergranular pores, lamellar illite interspersed with mud crystals of silica; (i) JH-6, Mud–crystal calcite crystal aggregates filled between relatively well-formed calcite crystals; (j) JH-22, mud crystal structure of rhodochrosite crystal assemblage with tight mosaic contact between rhodochrosite crystals; (k) JH-8, dolomite crystal aggregates and siliceous aggregates in a fine vein-like distribution; (l) JH-23, fine-grained structured calcite crystal aggregate in the form of fine veins, calcite veins flanked by siliceous veins.

In the silty mudstone, the grain type is predominantly quartz and feldspar, with a high content of rock fragments, subangular grains, poor sorting and roundness, and a primarily matrix-supported interstitial filling (Figure 3f,l). The authigenic minerals include calcite and siderite (Figure 3h,j). The quartz grains in some samples are laminated, forming a silty lamella (Figure 3d,f). Lithic chert occurs occasionally (Figure 3c), and a few samples contain heavy mineral detritus sphenite (Figure 3e).

XRD analysis of the whole rock showed that the main mineral components of fine-grained sediments in the Xu-3 Member are siliceous, clay, and carbonate minerals (Figure 4a) (Supplementary Materials Table S1). Some samples contain a large amount of siderites, and previous studies have shown that siderite is an important mineral for tracing the suboxide zone and methanogenic zone in sedimentary rocks [46]. Relevance analysis of whole rock XRD data showed that most samples have good correlation, indicating their similar geological background. However, the correlation varied considerably between a few samples, indicating differences in sedimentary environment or parent tectonic setting (Figure 4b).

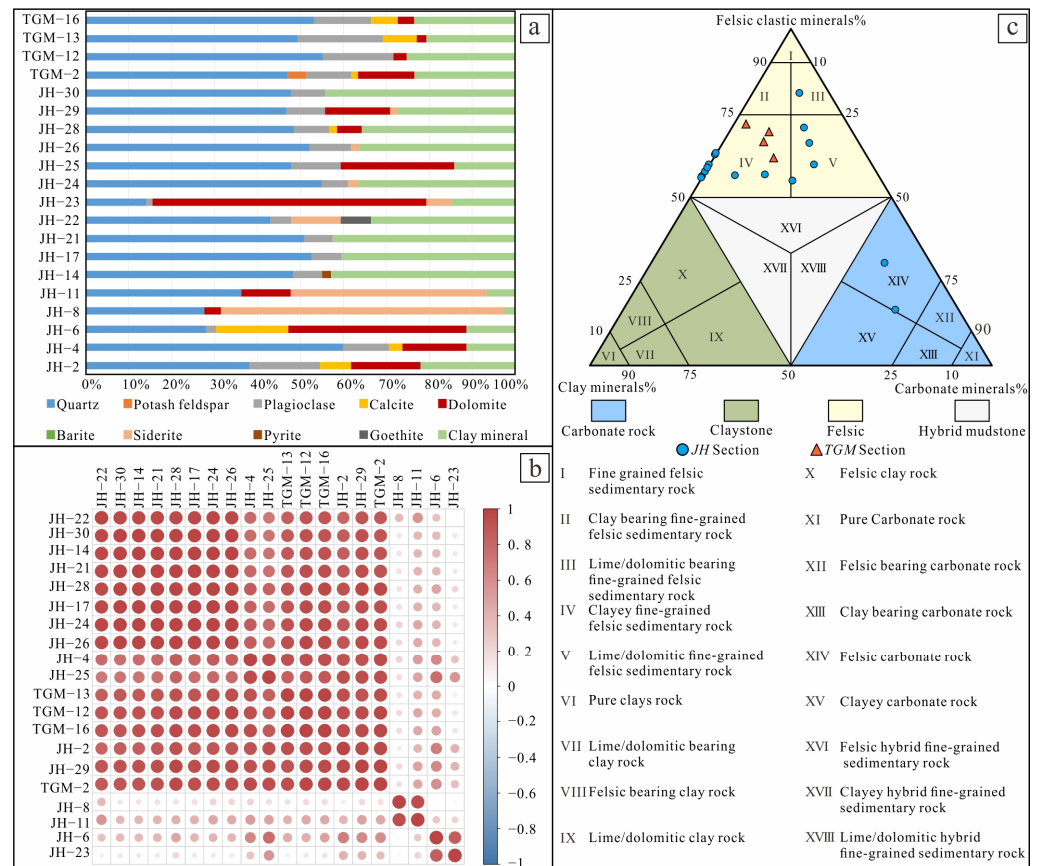


**Figure 4.** Mineralogical characteristics of fine-grained sedimentary rocks. (a) Mineralogical composition of fine-grained sedimentary rocks; (b) Correlation heat map of fine-grained sedimentary rocks; (c) Classification of mineral petrology.

The three-level nomenclature principle was used to determine the basic name of fine-grained sedimentary rocks [4], the total feldspathic clastic minerals, carbonate minerals, and clay minerals, which were further used as tri-terminal elements to classify the mineral composition of the Xu-3 Member. The results showed that the fine-grained sediments generally belong to the larger group of fine-grained felsic sedimentary rocks comprising clayey and lime fine-grained felsic sedimentary rocks (Figure 4c).

## 4.2. Geochemical Characteristics

### 4.2.1. Distribution of Major Elements

The major elements of the fine-grained sediments of the Xu-3 Member in the Western Sichuan Depression are generally characterized by high contents of  $\text{SiO}_2$  and  $\text{Al}_2\text{O}_3$ , and low contents of  $\text{MnO}$ ,  $\text{P}_2\text{O}_5$ , and  $\text{BaO}$ . Compared with standard mudstone (Supplementary Materials Table S2) [47], the average contents of  $^{\text{T}}\text{Fe}_2\text{O}_3$ ,  $\text{MnO}$ , and  $\text{MgO}$  for fine-grained sediments in the JH section are relatively high, while the average contents of  $\text{Al}_2\text{O}_3$ ,  $\text{Na}_2\text{O}$ , and  $\text{K}_2\text{O}$  are relatively low. Compared with the Post Archean Australian shale (PAAS), the fine-grained sediments have low contents of other elements, except  $\text{Al}_2\text{O}_3$  and  $\text{MnO}$  in the JH section; in the TGM section, the contents of  $\text{Al}_2\text{O}_3$ ,  $\text{Fe}_2\text{O}_3$ ,  $\text{MgO}$ ,  $\text{K}_2\text{O}$ ,  $\text{MnO}$ ,  $\text{TiO}_2$ , and  $\text{P}_2\text{O}_5$  are low, while the contents of  $\text{SiO}_2$  and  $\text{CaO}$  are high. Through PAAS standardized comparison of major element data [48],  $\text{TiO}_2$  was found to be depleted in most samples, while  $\text{CaO}$  is relatively enriched in almost all samples (Figure 5a).

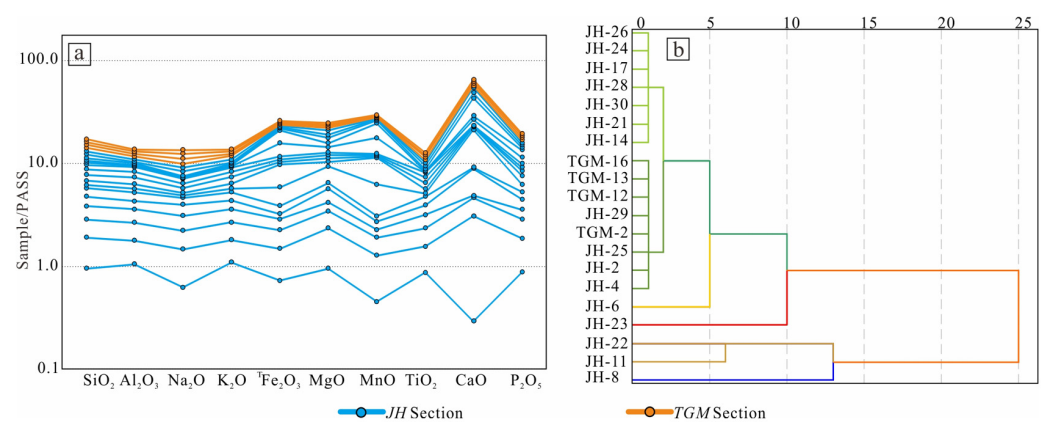


**Figure 5.** Characterization of the major elements of the Xu-3 Member in the JH and TGM sections (PAAS data from [48]). (a) PAAS standardization of fine-grained sedimentary rocks in the Xu-3 Member; (b) Cluster analysis of major elements of fine-grained sedimentary rocks in the Xu-3 Member.

According to the cluster analysis of the PAAS normalized data, most rocks could be classified into two main groups with relatively similar elemental characteristics, with the remaining individual rocks falling outside the main classification, which is consistent with the results of the previous correlation analysis of mineral composition. This indicates that the provenance or sedimentary environment influenced the formation of fine-grained sediments in the Xu-3 Member (Figure 5b).

### 4.2.2. Characteristics of Trace Elements and Rare Earth Elements

On the basis of the PAAS standardized trace element data [48], the fine-grained sediments of the Xu-3 Member exhibited distinct Sr depletion and relative enrichment of large ion lithophile elements (Rb, Ba, Th, U), high field strength elements (Zr, Hf), and La, Ce, and Y (Figure 6a) (Supplementary Materials Table S3).

PAAS was also used to standardize REEs [48], and the standardization diagram showed a gentle distribution pattern of REEs in the fine-grained sediments in the TGM section. REEs in the JH section in the north of the depression showed a gentle distribution with the enrichment of heavy REEs (Figure 6b) (Supplementary Materials Table S3).

Considering the relatively stable nature of REEs, their characteristics can generally indicate the tectonic background of the provenance [49]. Therefore, the different REE distribution patterns suggest that the fine-grained sediments in the Xu-3 Member may have different tectonic backgrounds and provenances.

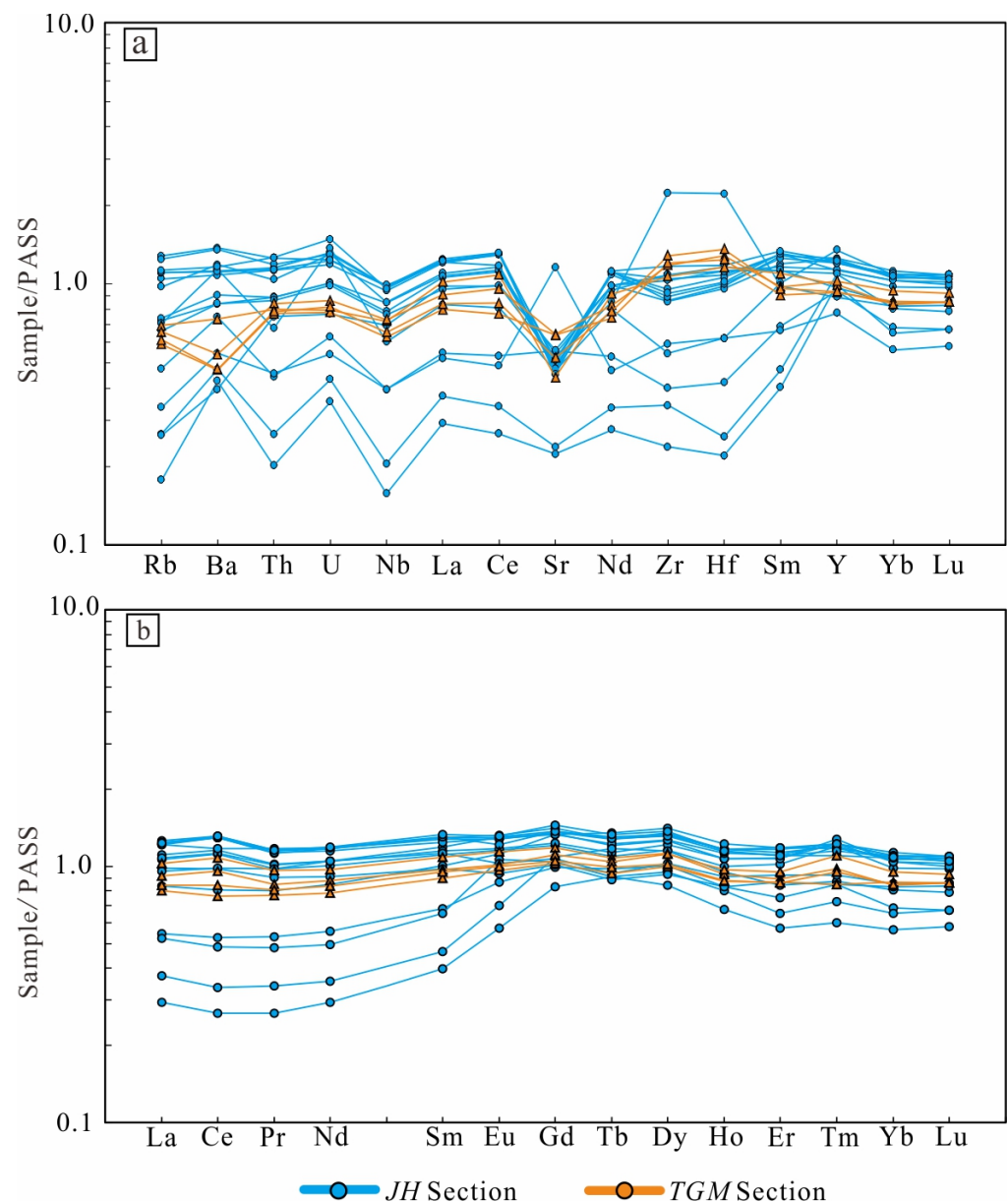


**Figure 6.** Characterization of trace elements and rare earth elements in the JH and TGM sections (PAAS data from [48]). (a) PAAS rock standardization chart of trace elements in the fine-grained sedimentary rocks of the Xu-3 Member; (b) PAAS standardization chart of REEs in the fine-grained sedimentary rocks of the Xu-3 Member.

#### 4.3. Total Organic Carbon Characteristics

The TOC contents in the Xu-3 Member display obvious variation through the JH section. The Xu-3 member is characterized by the lower TOC contents, ranging from 0.38 wt% to 4.62 wt% (mean = 2.37 wt%). The upper section is characterized by the higher TOC contents, ranging from 0.53 wt% to 4.62 wt% (mean = 2.76 wt%). The TOC contents of the lower section vary between 0.38 wt% and 3.85 wt% (mean = 1.87 wt%). The TOC content of TGM section ranges from 1.87 wt% to 3.26 wt% (mean = 2.35 wt%), and the change trend is consistent with JH section (Supplementary Materials Table S1). The described TOC profile is similar to those reported in previous studies of the Xu-3 Member [28,32].

#### 4.4. Data Validity Discrimination

REEs and some major elements are highly effective indicators of the original sedimentary environment [48,50]. However, some studies have shown that diagenesis can alter the distribution pattern of REEs, leading to Ce enrichment, Eu depletion, and a gradual decrease in the value of  $(La/Nd)_N$ , thus weakening the significance of REEs as indicators of the original sedimentary environment [51]. The manifestation is  $\delta Ce$ , and  $\delta Eu$  is well correlated with  $\Sigma REE$  [52].

The correlations between  $\delta Ce$ ,  $\delta Eu$  and  $\Sigma REE$ , and  $\delta Eu$  and  $(La/Nd)_N$  of the Xu-3 Member were analyzed. The results showed that  $\delta Eu$  is poorly correlated with  $\Sigma REE$ ,  $\delta Ce$  is not correlated with  $\delta Eu$ , and  $\delta Eu$  is not correlated with  $(La/Nd)_N$  (Figure 7). According to these results, the REE distribution in the study area was not influenced by later diagenesis and can therefore be used to indicate the original depositional environment. However, several samples (JH-2, JH-6, JH-23, and JH-25) with high dolomite content may not be used to analyze the sedimentary environment temporarily due to the influence of diagenesis. Therefore, these samples will be removed in subsequent analyses.

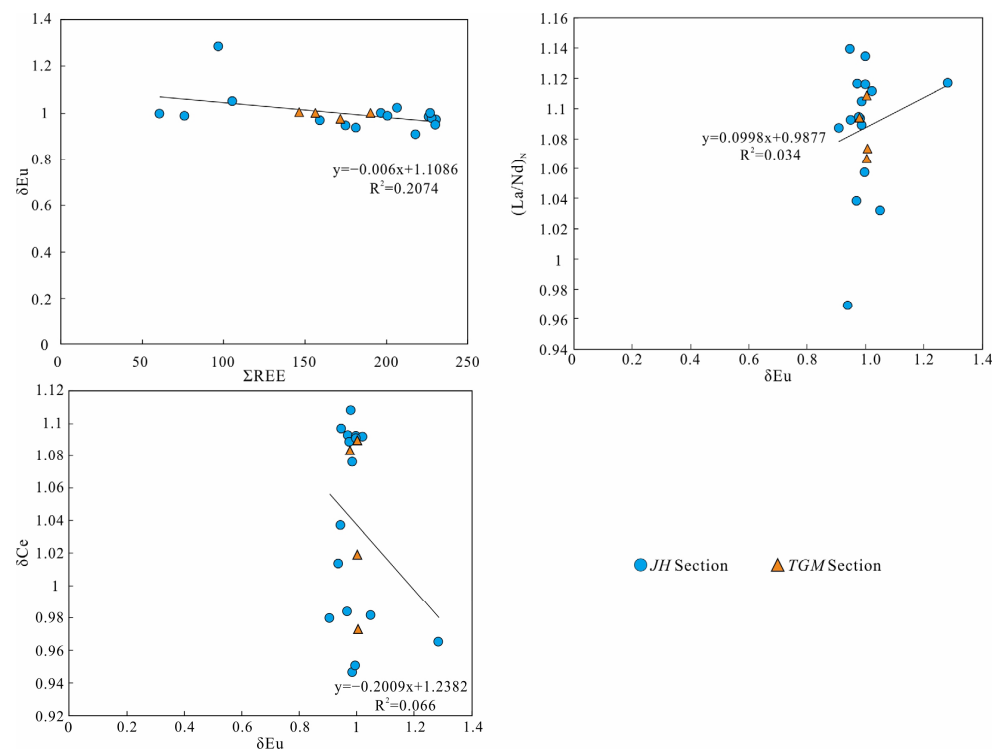


**Figure 7.** Data validity discrimination diagram of the JH and TGM sections.

## 5. Discussion

### 5.1. Paleoclimate and Paleo-Productivity

According to previous studies on palynoflora, the majority of pteridophytes are warm, it is inferred that the climate of the Sichuan Basin was warm and humid during the deposition of the Xujiahe Formation in the Late Triassic, belonging to the tropical–subtropical climate [53,54]. On this basis, this study will use geochemical methods to analyze the paleoclimate characteristics of the sedimentary period of the Xu-3 Member of the Xujiahe Formation in the Western Sichuan Depression.

Sediments in humid environments are enriched in Fe, Mn, Cr, V, Ni, and Cu, whereas they are relatively enriched in Ca, Mg, K, Na, Sr, and Ba under arid conditions [55]. The ratio of arid conditions elements Sr (arid conditions) to Cu and Cr (humid conditions) can effectively reflect the paleoclimate [56]. Sr/Cu ratios greater than five and a large Sr/Cr ratio indicate a dry and hot climate, while the opposite is true for a warm and humid

climate [57,58]. The change of REEs is also related to climate change. Increasing REE contents generally indicate that the climate changed from arid to humid [59].

In the JH section of the Western Sichuan Depression, the Sr/Cu and Sr/Cr ratios are higher at the bottom and middle upper parts, and lower at the middle lower part and top, indicating a paleoclimate transition from hot–arid to warm–humid (Figure 8a,b). In the north and central parts of the depression, Sr/Cu and  $\Sigma$ REEs show a good negative correlation (Figure 9a). Sr/Cu and Sr/Cr show a good positive correlation (Figure 9b) and Sr/Cr and  $\Sigma$ REE show a negative correlation (Figure 9c). The TGM section in the central part of the depression had a warm and humid climate, while the southern LCG section experienced a transition from a humid climate to a dry and hot climate (Figure 9).

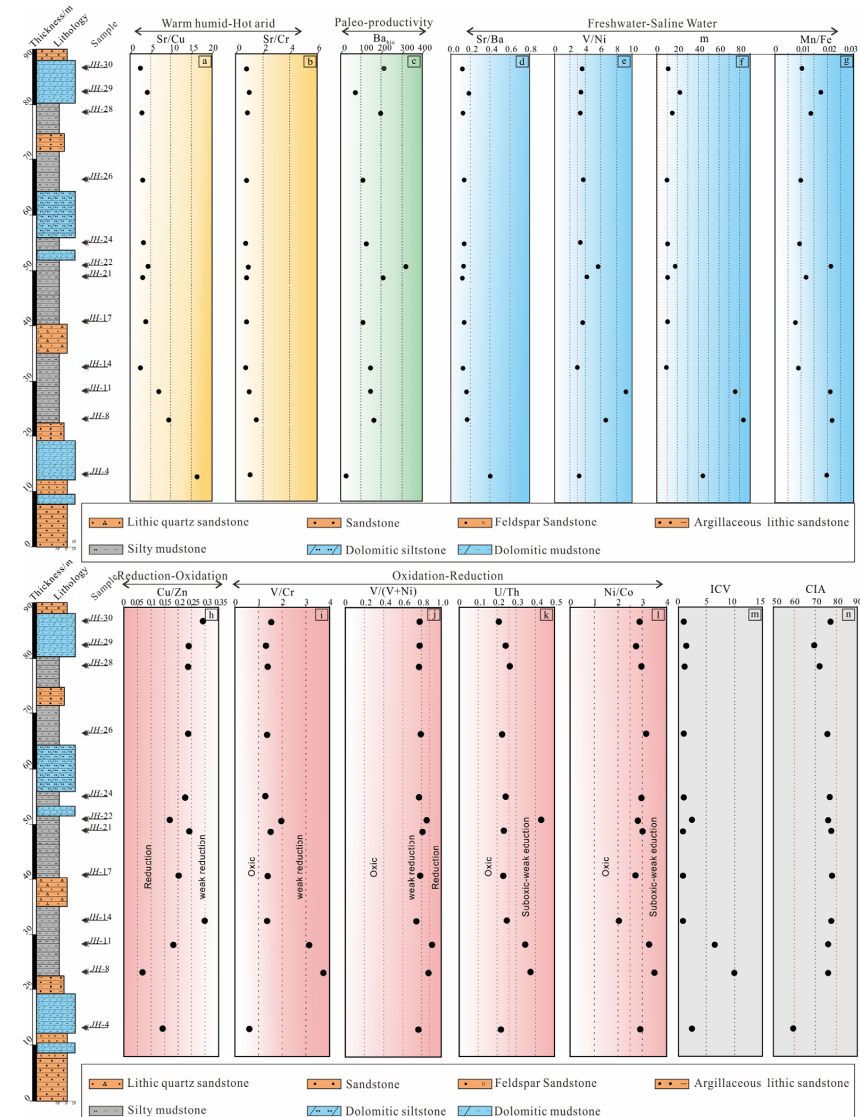


**Figure 8.** Profiles of paleoclimatic (Sr/Cu and Sr/Cr), paleo-productivity ( $Ba_{bio}$ ), paleo-salinity (Sr/Ba, V/Ni, m, and Mn/Fe), paleo-redox (Cu/Zn, V/Cr, V/(V + Ni), U/Th, and Ni/Co) and chemical weathering degree (ICV and CIA) changes in the JH section of the Xu-3 Member. (a,b) Change trend of the paleoclimate in the JH section; (c) Change trend of paleo-productivity  $Ba_{bio}$  in the JH section. (d) Change trend of Sr/Ba in paleo-salini; (e) Change trend of V/Ni in paleo-salinity; (f) Change trend of m in paleo-salinity; (g) Change trend of Mn/Fe in paleo-salinity; (h) Change trend of Cu/Zn in paleo-redox; (i) Change trend of V/Gr in paleo-redox; (j) Change trend of V/(V + Ni) in paleo-redox; (k) Change trend of U/Th in paleo-redox; (l) Change trend of Ni/Co in paleo-redox; (m) Change trend of ICV in chemical weathering degree; (n) Change trend of CIA in chemical weathering degree.

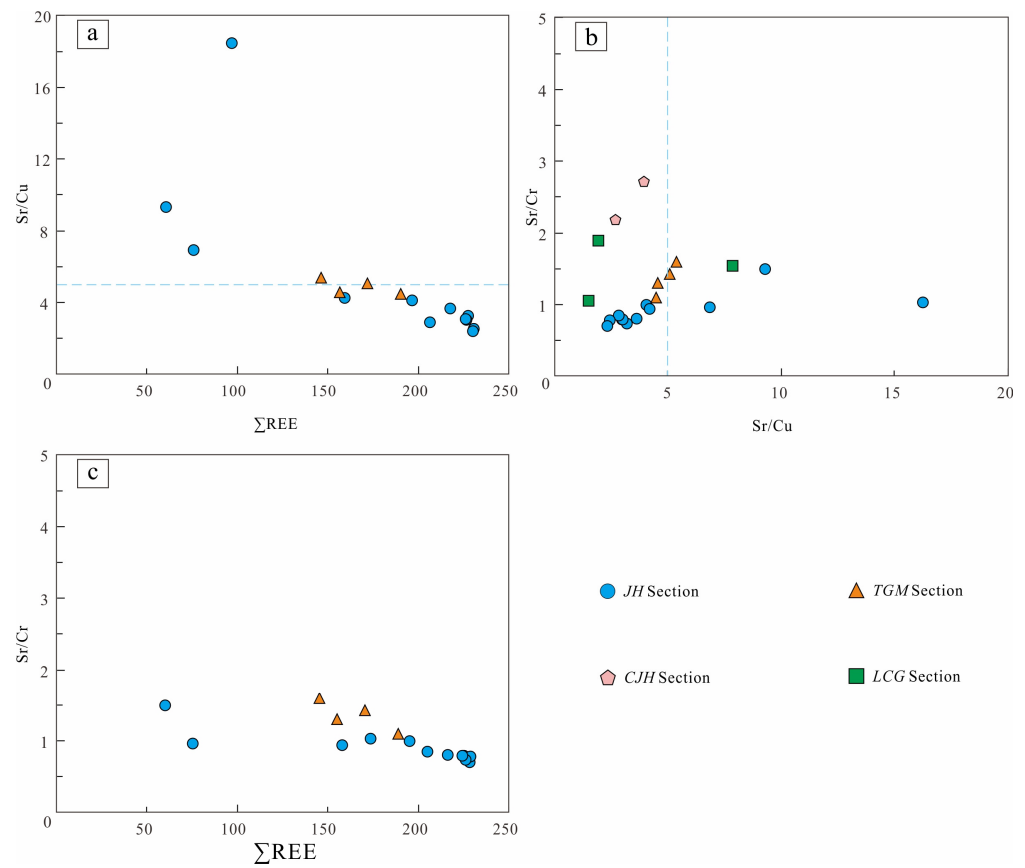


**Figure 9.** Diagrams of paleoclimatic and paleo-productivity changes in the Xu-3 Member. (a) Sr/Cu-REE correlation diagram; (b) Sr/Cr-REE correlation diagram; (c) Sr/Cu-Sr/Cr correlation diagram (CJH and LCG data from [32]).

Therefore, the paleoclimate during the sedimentary period of the fine-grained sediments in the Xu-3 Member was characterized by a transformation from hot–arid to warm–humid from bottom to top, and the paleoclimate in the south and central parts of depression was drier and hotter than that in the north.

The content of Ba, which primarily originates from the input of terrigenous detritus and biological sources, can effectively indicate the paleo-productivity of surface water [60,61]. Therefore, biological barium ( $Ba_{bio}$ ) is considered a reliable indicator of paleo-productivity; it can be obtained by subtracting terrestrial Ba content from total Ba content sediments [62,63].

The  $Ba_{bio}$  of the fine-grained sediments the Xu-3 Member exhibited distinct changes, and the ratio of  $Ba_{bio}$  to Sr/Cu and Sr/Cr showed a good consistency, indicating that the change of paleoclimate had a certain control over the paleo-productivity (Figure 8c). However, the  $Ba_{bio}$  content in the middle and south of the depression was extremely low, and even to negative in some sections (Supplementary Materials Table S4). As the contents of  $TiO_2$ ,  $Al_2O_3$ , and Zr can reflect the input of detritus from the continental margin, higher contents of these substances generally indicate a larger input of detritus from the continental margin [64]. The contents of these three substances were higher in the TGM and LCG sections of the depression than in the JH section (Supplementary Materials Table S4). These characteristics indicate that the input of terrigenous detritus was large in the TGM and LCG sections, which were a low-density, biologically weak zone, thus resulting in low paleo-productivity. In addition, the JH section belongs to a higher density biological large zone, thus resulting in large paleo-productivity.

### 5.2. Paleo-Salinity Analysis

The ratios of Sr/Ba, Mn/Fe, and V/Ni are commonly used to determine the water salinity during the sedimentary period. In general, Sr/Ba < 0.6, indicates brackish water to fresh water conditions; ratios between 0.6 and 1 indicate brackish water conditions; and Sr/Ba > 1 indicates saline water conditions. For marine salt water, the Mn/Fe ratio is high, and V/Ni > 3. For continental fresh water, the Mn/Fe ratio is low and V/Ni < 3 [65,66].

Considering that Al<sub>2</sub>O<sub>3</sub> is mainly supplied by continental sources and MgO originates from marine sources, the paleo-salinity of sedimentary water can be analyzed by the ratio “m” of Mg to Al [11,67]. In a transitional sedimentary environment from fresh water to sea water, the value of “m” increases with increasing salinity in the sedimentary environment: m < 1 indicates freshwater sedimentary environments; m between 1 and 10 indicates transitional sedimentary environments between sea and land; and m > 10 indicates seawater sedimentary environments [68,69].

In this study, a distinct variation of paleo-salinity was observed in the JH section (Figure 8d–g). This change is also consistent with the previous results of changes in paleoclimate and paleo-productivity. This indicates that the northern part of the Western Sichuan Depression was dominated by brackish water to saline water during sedimentation.

The Sr/Ba and Mn/Fe ratios of the TGM and LCG sections in the south and central parts of the depression were low, indicating low paleo-salinity (Figure 10a,b). This shows that the sedimentary waters in the middle and southern depression were mainly brackish water, with lower salinity than that in the northern part.

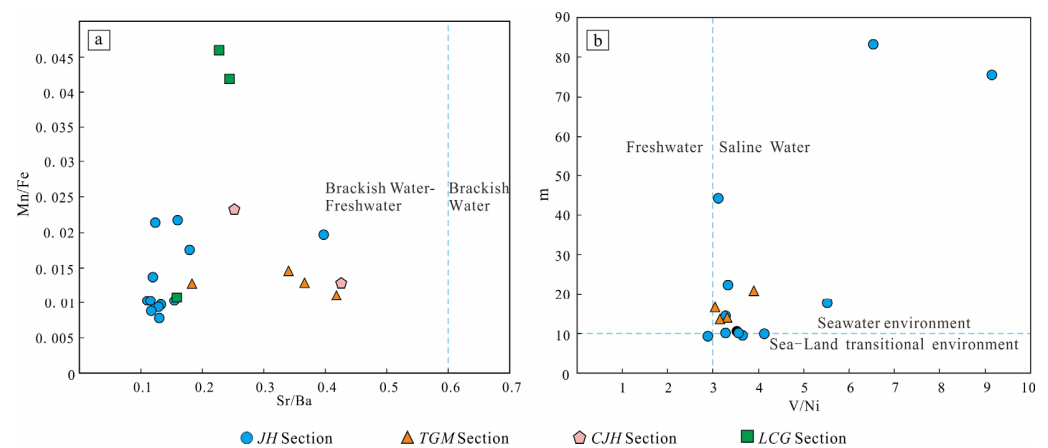


**Figure 10.** Diagrams of paleo-salinity changes in the Xu-3 Member (CJH and LCG data from [32]). (a) Sr/Ba-Mn/Fe correlation diagram; (b) V/Ni-m correlation diagram.

Therefore, the paleo-salinity of water during the sedimentation of the fine-grained sediments in the Xu-3 Member was generally a mixture of saline water and fresh water, but the salinity was lower in the middle and southern parts than in the northern part. This difference in salinity may be related to the input of the terrigenous clasts mentioned above.

Dai Chaocheng et al. (2018) restored the paleo-salinity of the Xujiache Formation through the calculation of boron content and clay mineral composition. The overall salinity is between 4.8‰ and 19.7‰, with an average of 12.8‰, which is far lower than the normal seawater salinity [70]. Based on the analysis of Li, Sr, Ni, and Ga element contents, Lai Wei (2019) judged that the Xujiache Formation in the Eastern Sichuan Basin belongs to the freshwater–brackish water sedimentary environment [71]. It shows that the previous research is consistent with the research results of this study.

### 5.3. Paleo-Redox Conditions

The paleo-redox conditions indicate the extent to which the rocks were affected by oxidation and reduction in the process of sedimentation and reflect the sealing conditions in the sedimentary period [72]. The enrichment or depletion of Cu, Zn, V, Ni, U, Th, and

other elements will change under the influence of paleo-redox conditions; therefore, the paleo-redox conditions can be analyzed through the geochemical ratios of related elements based on the characteristics of available elements [47,55,73,74].

According to the paleo-redox conditions of the fine-grained sediments of the JH Section, most of the samples were deposited in a sub-oxidative to sub-reductive environment (Figure 8h–l). This trend is consistent with the changes in paleoclimate, paleo-productivity, and paleo-salinity described above. Considering the formation environment of siderite [46], the occurrence of siderite in the fine-grained sediments of the JH section indicates a weakly reducing environment during a part of the sedimentation of the Xu-3 Member.

In a redox correlation plot with the Cu/Zn ratio as the X-axis and several other parameters as the Y-axis, the redox conditions of the fine-grained sediments generally correspond to sub-oxidation to sub-reduction, with a few samples being deposited under oxidation conditions in the TGM and LCG sections of the central and southern part of the depression (Figure 11a,d).

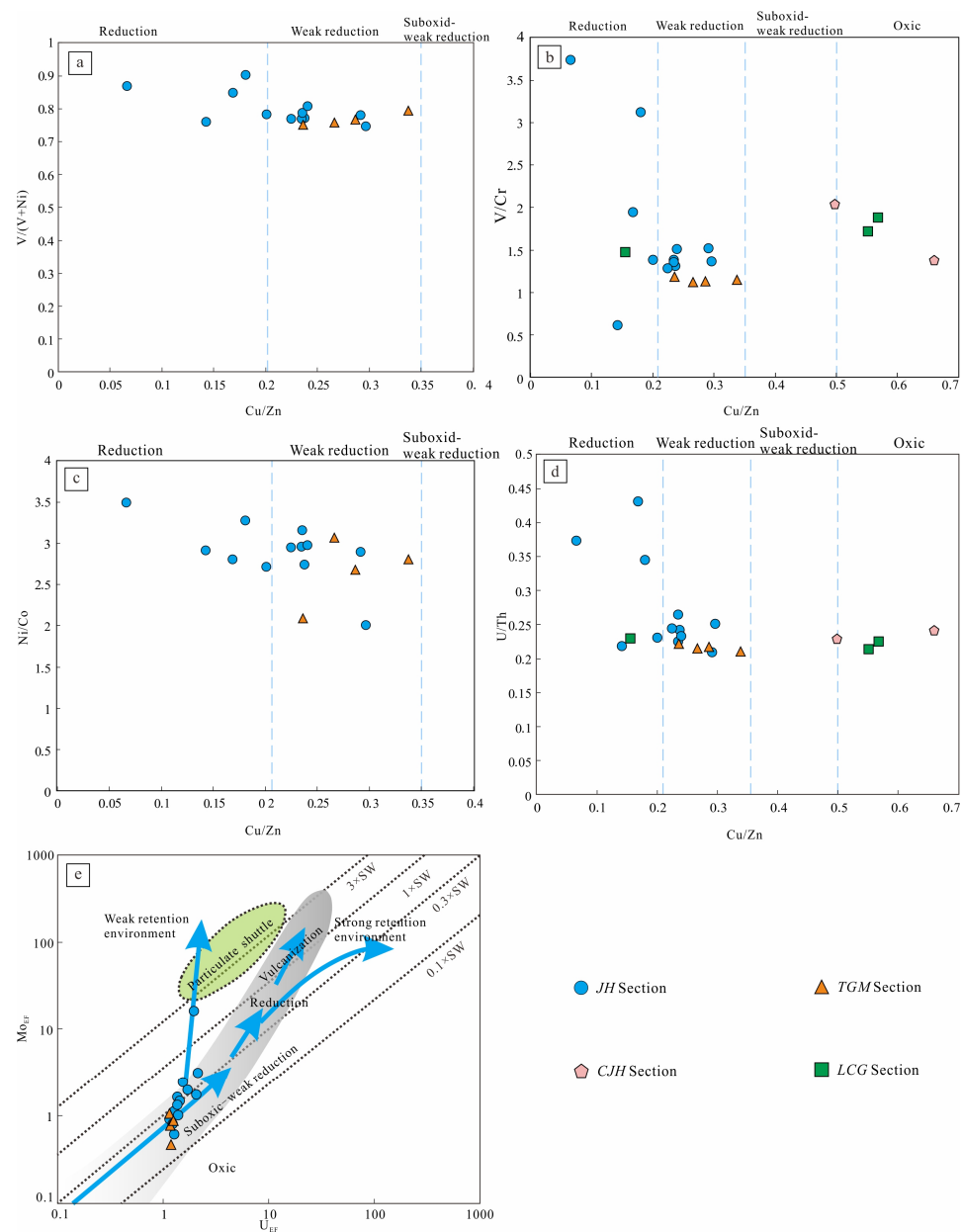


**Figure 11.** Discrimination map of the redox environment of each section in the Xu-3 Member (CJH and LCG data from [32]). (a) V/(V + Ni)-Cu/Zn; (b) V/Cr-Cu/Zn; (c) Ni/Co-Cu/Zn; (d) U/Th-Cu/Zn;

(e) of the  $U_{EF} - Mo_{EF}$  (after [75,76]; revised). The molar concentration ratio of Mo/U in standard seawater is represented by  $1 \times SW$ ;  $3 \times SW$ ,  $0.3 \times SW$ , and  $0.1 \times SW$  indicate Mo/U ratios 3 times, 0.3 times, and 0.1 times that of standard seawater, respectively. The grey area represents the U-Mo covariant model in a normal open marine environment, and the green area represents the U-Mo covariant model under the action of metal particle carriers.

The enrichment factor (EF) of some trace elements can also be used to discriminate the redox conditions in waters during the deposition period, such as  $U_{EF}$  and  $Mo_{EF}$  [75,76], and element enrichment factors ( $EF_{element}$ ) are determined using the formula:

$$EF_{element} = (\text{element}/Al)_{\text{sample}} / (\text{element}/Al)_{\text{average shale}} \quad (1)$$

According to the  $U_{EF}$  and  $Mo_{EF}$  correlation diagram, the fine-grained sediments of the Xu-3 Member were generally under suboxic to weak reduction conditions (Figure 11e).

Previous studies on the paleo-redox conditions of the mudstone of the Xujiahe Formation in the eastern Sichuan Basin show that the sedimentary water in this period is a reducing condition as a whole; the reducibility of the water from the first to the fifth member of the Xujiahe Formation is gradually weakened; and the oxidizability is gradually enhanced [71]. The study of the paleo-redox conditions of the Xu-3 Member of the Xujiang Formation shows that this change also exists in the western Sichuan depression.

#### 5.4. Chemical Weathering Degree

The degree of rock weathering is affected by the parent rock, paleoclimate, and tectonic environment [77–79]. The index of compositional variation (ICV) and chemical index of alteration (CIA) are commonly used to assess the intensity of chemical weathering in clastic sediment provenance areas.

ICV is usually used to determine whether clastic rocks directly formed from the first deposition of parent materials or from recycled sediments [80–82]. ICV values higher than 1 indicate compositional immaturity of clastic rocks, reflecting the first cycle of deposition in a tectonically active area [49]. ICV values lower than 1 indicate high compositional maturity of clastic rocks, reflecting the recycling of sedimentary materials or the first deposition under strong chemical weathering [83,84]. The calculation formula is shown in Table 1.

**Table 1.** Summary of chemical weathering indices and their computational formulae.

No.	Index	Formula	References
1.	CIA: Chemical Index of Alteration	$= Al_2O_3 / (Al_2O_3 + Na_2O + K_2O + CaO^*) \times 100$	Nesbitt et al. [85]
2.	ICV: Index of Compositional Variability	$= (Fe_2O_3 + K_2O + Na_2O + CaO + MgO + MnO + TiO_2) / Al_2O_3$	Cox et al. [86]

The oxide parameters in the formula are in moles,  $CaO^*$  in the table refers to  $CaO$  in silicate minerals. When the  $CaO$  content in silicate minerals cannot be obtained separately, it is necessary to correct the  $CaO$  content. The  $CaO^*$  is calculated using the method proposed by McLennan [48],  $CaO_{surplus} = CaO - P_2O_5 \times 10/3$ , If calculated  $CaO_{surplus} < Na_2O$ ,  $CaO^* = CaO_{surplus}$ ; If calculated  $CaO_{surplus} > Na_2O$ ,  $CaO^* = Na_2O$ .

In this study, the ICV index of most fine-grained sediments were higher than 1, and they can thus be determined to be from the first deposition during tectonic activity (Figure 8m). Nevertheless, the recycling status of some samples with  $ICV < 1$  requires further confirmation.

Sediment sorting and recycling will lead to differentiation, which promotes the enrichment of heavy minerals in sediments. Trace elements Th, Sc, and Zr generally exist in different types of rocks; they are chemically stable during deposition and do not undergo fractionation [48]. The Zr/Sc ratio can represent the degree of recycling, and the Th/Sc ratio does not change with sediment recycling. Therefore, the composition change, sorting degree, and degree of heavy mineral enrichment of sediments can be assessed using these ratios [87].

In the Th/Sc-Zr/Sc cross plot (Figure 12a), the fine-grained rocks are relatively close to the composition evolution line. The composition of almost all fine-grained rocks is mainly controlled by the rock composition of the provenance, indicating that sedimentary recycling has little impact on them.

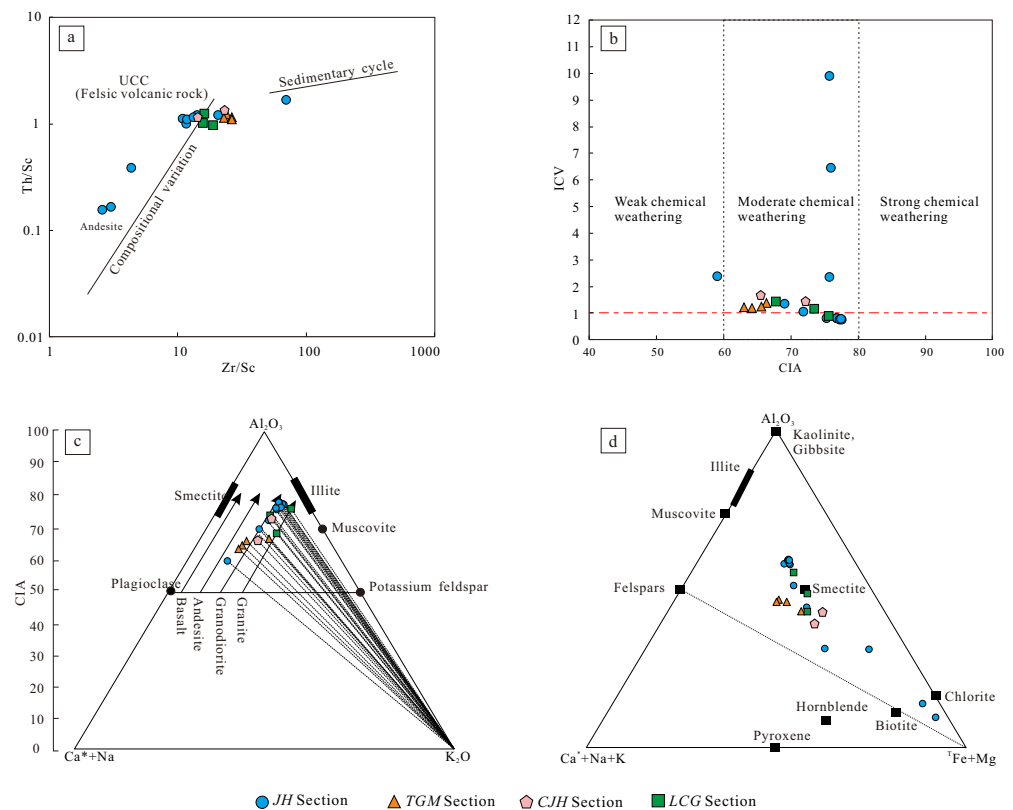


**Figure 12.** Discrimination map of the chemical weathering degree of the Xu-3 Member. (a) ICV-CIA related diagrams; (b) Th/Sc-Zr/Sc diagrams (after [88]); (c) A-CN-K diagrams (after [89]); (d) A-CN-K-FM diagrams (after [77]) (CJH and LCG data from [32]).

CIA can indicate the chemical weathering intensity and paleoclimate of the provenance area, but the influence of recycling must be excluded before CIA analysis. CIA values between 50 and 60 indicate weak chemical weathering under cold and dry climatic conditions; CIA values ranging from 60 to 80 indicate moderate weathering under warm and humid climate conditions; and CIA values ranging from 80 to 100 indicate strong weathering under hot and humid subtropical climate conditions [85–92]. The CIA of fine-grained sediments in the Xu-3 Member ranged from 60 to 80 (Figures 8n and 12a), reflecting moderate chemical weathering under a warm and humid climate in the provenance area (Figure 12b).

After calculating the CIA value, the A-CN-K diagram can be used to distinguish the parent rock composition in the provenance area [89–93]. Basalt, andesite, granodiorite, granite, and other important bedrock types are projected in corresponding positions in the A-CN-K diagram according to chemical composition. The parent rocks of fine-grained sediments are mainly felsic rocks, but the parent rocks were not completely identical between the northern and south-central parts of the depression (Figure 12c).

On this basis, Nesbitt and Young (1984) [90] further proposed the A-CN-K-FM ( $\text{Al}_2\text{O}_3 - \text{CaO}^* + \text{Na}_2\text{O} + \text{K}_2\text{O} - \frac{1}{2}\text{Fe}_2\text{O}_3 + \text{MgO}$ ) triangle model diagram of the weathering trends of light-colored minerals and dark colored minerals. Some fine-grained sediments of the Xu-3 Member in the A-CN-K-FM diagram tend towards the dark mineral direction, indicating that the parent rock type of these rocks may be more neutral (Figure 12d).

### 5.5. Depositional Pattern

Based on the petrological description and geochemical analysis, the depositional pattern of the Xu-3 Member was established (Figure 13). During the deposition of the Xu-3 Member, the fine-grained sediments in the central and southern regions of the depression (TGM and LCG sections) were deposited in a shallow freshwater lake within an oxygen-rich and relatively arid and hot paleoclimate, which may indicate that the depositional environment received large input from the continental margin. In contrast, the fine-grained sediments in the northern part of the depression (JH section) were deposited in a large, deep, and brackish water–saline water lake with sub-oxidative to sub-reductive conditions under and a relatively warm, humid paleoclimate. This indicates that although the JH section lies to the north of the depression, it was the depocenter of the lake.

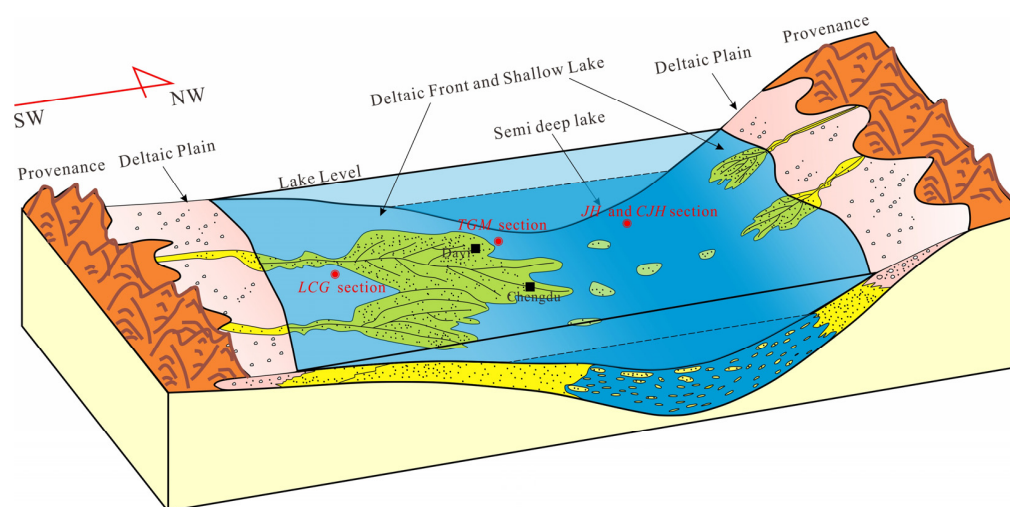


**Figure 13.** Depositional pattern of the Xu-3 Member in the Western Sichuan Depression, SW China.

The Western Sichuan Depression received material supply from various provenance areas. The provenance and depositional areas were in close proximity and had similar climates, but the parent rock types were not identical.

### 6. Conclusions

- (1) The composition of fine-grained sediments in the Xu-3 Member of the Western Sichuan Depression can be classified into two main types of fine-grained felsic sedimentary rocks: clayey and lime fine-grained felsic sedimentary rocks. The Xu-3 Member is characterized by lower TOC contents.
- (2) According to the characteristics of major elements, most rocks can be divided into two similar categories. Among trace elements, large ion lithophile elements and high field strength elements are relatively enriched. The REE distribution pattern of the TGM section is gentle, while the Jinhe section has two types of patterns: gentle and heavy REEs enrichment type.
- (3) The paleoclimate experienced a transition from hot–arid to warm–humid, and it was hotter in the central and southern parts of the depression than in the northern part. The paleo-productivity was consistent with the change trend of the paleoclimate, with relatively low levels in the central and southern parts of the depression, which may be related to the higher input of debris from the continental margin. The paleo-salinity primarily reflected brackish water to saline water, with fresh water injection in the southern part of the depression. The paleo-redox conditions of the waters were sub-oxidation to sub-reduction types.
- (4) The degree of chemical weathering in the provenance area was moderate, and the paleoclimate was warm and humid, essentially consistent with the sedimentary area.

The parent rock type was mainly felsic rocks, but they were not completely identical between the northern and south-central parts of the depression.

**Supplementary Materials:** The following supporting information can be downloaded at: <https://www.mdpi.com/article/10.3390/min13040510/s1>, Table S1: XRD and TOC; Table S2: Major elements; Table S3: Trace elements and REEs; Table S4: Calculated data.

**Author Contributions:** Conceptualization, J.T. and Y.L.; methodology, Q.L.; data curation, X.L.; writing—original draft preparation, Y.L. and X.L.; writing—review and editing, J.T. and Q.L.; All authors have read and agreed to the published version of the manuscript.

**Funding:** This work was supported by the National Science Foundation of China (Projects 42172135).

**Data Availability Statement:** Data will be made available on request.

**Acknowledgments:** The careful reviews and constructive suggestions of the manuscript by anonymous reviewers are greatly appreciated.

**Conflicts of Interest:** The authors declare no conflict of interest.

## References

1. Potter, P.E.; Maynard, J.B.; Depetris, P.J. *Mud and Mudstone*; Springer Verlag: Berlin, Germany, 2005; pp. 1–297.
2. Aplin, A.C.; Macquaker, J.H.S. Mudstone diversity: Origin and implications for source, seal, and reservoir properties in petroleum systems. *AAPG Bull.* **2011**, *95*, 2031–2059. [[CrossRef](#)]
3. Liu, H.M.; Sun, S.Y.; Cao, Y.C.; Liang, C.; Zhang, C.C. Lithofacies characteristics and distribution model of fine-grained sedimentary rock in the lower Es3 member, Dongying Sag. *Petro. Geol. Recovery Effic.* **2017**, *24*, 1–10. [[CrossRef](#)]
4. Peng, J.; Zeng, Y.; Yang, Y.M.; Yu, L.T.; Xu, T.Y. Discussion on classification and naming scheme of fine-grained sedimentary rocks. *Pet. Explor. Dev.* **2022**, *49*, 121–132. [[CrossRef](#)]
5. Jiang, Z.X.; Zhang, W.Z.; Liang, C.; Wang, S.Y.; Liu, H.M.; Chen, X. Characteristics and evaluation elements of shale oil reservoir. *Acta Pet. Sin.* **2014**, *35*, 184–196. [[CrossRef](#)]
6. Li, Y.; Liu, K.Y.; Pu, X.G.; Chen, S.Y.; Han, W.Z.; Zhang, W.; Wang, H.; Liang, C.; Zhao, J.H. Lithologic characteristics and Formation environments of mixed fine-grained sedimentary rocks in second member of Kongdian Formation in Cangdong Depression, Bohai Bay Basin. *Earth Sci. China Univ. Geosci.* **2020**, *45*, 3779–3796. [[CrossRef](#)]
7. Loucks, R.G.; Ruppel, S.C. Mississippian Barnett Shale: Lithofacies and depositional setting of a deep-water shale-gas succession in the Fort Worth Basin, Texas. *AAPG Bull.* **2007**, *91*, 579–601. [[CrossRef](#)]
8. Armstrong-Altrin, J.S. Evaluation of two multidimensional discrimination diagrams from beach and deep-sea sediments from the Gulf of Mexico and their application to Precambrian clastic sedimentary rocks. *Int. Geol. Rev.* **2015**, *57*, 1446–1461. [[CrossRef](#)]
9. Babu, K. Geochemical characteristics of sandstones from cretaceous Garudamangalam Area of Ariyalur, Tamilnadu, India: Implications of provenance and tectonic setting. *J. Earth Syst. Sci.* **2017**, *126*, 45. [[CrossRef](#)]
10. Liang, Q.S.; Tian, J.C.; Zhang, X.; Sun, X.; Yang, C.Y. Elemental geochemical characteristics of lower-middle Permian mudstones in Taikang Uplift, Southern North China Basin: Implications for the FOUR-PALEO conditions. *Geosci. J.* **2020**, *24*, 17–33. [[CrossRef](#)]
11. Lin, X.W.; Zhang, Z.K.; Liu, X.D.; Chen, N.; Wu, T.; Zhang, Y.F.; Zhao, P.B.; Ma, X.Q.; Zhou, Z.Z. Geochemical characteristics of Late Triassic sandstones in the western part of Bayan Har Basin, Northern Tibetan Plateau, Western China: Constraints on provenance, source weathering, tectonic setting, and paleoenvironment. *Geol. J.* **2020**, *55*, 5275–5293. [[CrossRef](#)]
12. Chen, X.L.; Ji, Y.L.; Yang, K.M. Sedimentary Characteristics Within Sequence Stratigraphic Framework of the Fourth Member of Xujiahe Formation in Middle Area of Western Sichuan Depression. *J. Jilin Univ. Earth Sci. Ed.* **2020**, *50*, 1615–1627. [[CrossRef](#)]
13. Huang, J.L.; Zou, C.N.; Li, J.Z.; Dong, D.Z.; Wang, S.L.; Wang, S.Q.; Cheng, K.M. Shale gas generation and potential of the Lower Cambrian Qiongzhusi Formation in the Southern Sichuan Basin, China. *Pet. Explor. Dev.* **2012**, *39*, 75–81. [[CrossRef](#)]
14. Li, S.F.; Wang, S.L.; Bi, J.X.; Zeng, Z.Q.; He, Y.M. Characteristics of Xujiahe Formation source rock and process of hydrocarbon-generation evolution in Puguang Area. *Earth Sci.* **2016**, *41*, 843–852.
15. Yu, Y.; Lin, L.B.; Nan, H.L. Trace and rare-earth element characteristics of fine-grained sediments in the Upper Triassic Xujiahe Formation in the western Sichuan Basin, SW China: Implications for the provenance and depositional environment. *Carbonates Evaporites* **2021**, *36*, 1–13. [[CrossRef](#)]
16. Xu, Z.H.; Hu, S.Y.; Wang, Z.C. Restoration of Paleoclimate and Its Geological Significance: As an Example from Upper Triassic Xujiahe Formation in Sichuan Basin. *Acta Sedimentol. Sin.* **2011**, *29*, 235–244.
17. Chen, D.X.; Liu, Y.C.; Pang, X.Q. Reservoir characteristics and its control on gas bearing properties of the 5th Member of the Triassic Xujiahe Formation continental shale in the Sichuan Basin of China. *Earth Sci. Front.* **2016**, *23*, 174–184.
18. Chen, Y.; Liu, S.G.; Li, Z.W.; Deng, B.; Zeng, X.L.; Lin, J. LA-ICP-MS detrital zircon U-Pb geochronology approaches to the sediment provenance of the Western Sichuan Foreland Basin and limited uplift of the Longmen Mountains during the early stage of Late Triassic. *Geotecton. Et Metallog.* **2011**, *35*, 315–323. [[CrossRef](#)]

19. Dai, Z.C.; Zheng, R.C.; Ren, J.P.; Zhu, R.K. Provenance analysis of Xujiahe Formation of Upper Triassic in Sichuan Foreland Basin and its geology implications. *J. Jilin. Univ. Earth Sci. Ed.* **2014**, *44*, 1085–1096. [[CrossRef](#)]
20. Shao, T.B.; Cheng, N.F.; Song, M.S. Provenance and tectonic-paleogeographic evolution: Constraints from detrital zircon U-Pb ages of Late Triassic-Early Jurassic deposits in the Northern Sichuan Basin, Central China. *J. Asian Earth Sci.* **2016**, *127*, 12–31. [[CrossRef](#)]
21. Fu, Z.K.; Wang, X.L.; Song, R.Q.; Xu, W.; Zhuo, J.C.; Zhang, L.; Yi, J.D. The characteristics and main controlling factors of high-quality tight sandstone reservoir in the 3th Member of Xujiahe Formation in West Sichuan Depression. *Geol. China.* **2022**, *49*, 298–310.
22. Pan, K. Characteristic and Controlling Effect on Natural Gas Accumulating of Xujiahe Formation Source Rock in Northeast Sichuan Basin. *Sch. Geosci. China Univ. Pet. East China* **2019**. [[CrossRef](#)]
23. Wu, X.Q.; Chen, Y.B.; Liu, Q.Y.; Wang, P.; Zeng, H.S.; Wang, Y.Q.; Hu, Y.; Li, H.J. Molecular geochemical characteristics of source rocks in the 5th Member of Upper Triassic Xujiahe Formation, Xinchang Gas Field, West Sichuan Depression. *Earth Sci. China Univ. Geosci.* **2019**, *44*, 859–871. [[CrossRef](#)]
24. Xu, H.; Liu, M.J.; Zhang, Z.; Ye, S.J.; Yang, Y.T.; Wu, L.; Nan, H.L.; Tan, X.C.; Zeng, W.; Lian, C.B. Diagenesis and porosity evolution of the 3rd Member of Xujiahe Formation tight sandstone reservoir in Western Sichuan depression, Sichuan Basin. *Nat. Gas. Geosci.* **2022**, *33*, 344–357.
25. Huang, L.S.; Yan, J.P.; Liu, M.J.; Zhang, Z.; Ye, S.J.; Zhang, F.; Zhong, G.H.; Wang, M.; Wang, J.; Geng, B. Diagenetic facies logging identification and application of deep tight sandstone gas reservoir: A case study of the Third member of Xujiahe Formation in Dayi area of western Sichuan depression. *J. China Univ. Min. Technol.* **2022**, *51*, 107–123. [[CrossRef](#)]
26. Wang, L.H.; Zhao, H.; Wu, L.; Tian, J. Geochemical characteristics of hydrocarbon source rock of the member 3 of Xujiahe Formation in the south area of Langzhong, Sichuan, China. *J. Chengdu Univ. Technol. Sci. Technol. Ed.* **2020**, *47*, 169–177. [[CrossRef](#)]
27. Ye, S.J.; Yang, Y.T.; Zhang, L. Characteristics and distribution of “sweet spot” reservoirs in the third and fifth members of Upper Triassic Xujiahe Formation, Western Sichuan Depression, Sichuan Basin. *Oil Gas Geol.* **2021**, *42*, 829–840, 862. [[CrossRef](#)]
28. Chen, B.; Li, Y.; Wang, W.M.; Li, H.B.; Su, D.C.; Yan, Z.K. The Provenance and Tectonic Setting of Late Triassic Xujianhe Formation in the Longmenshan Foreland Basin, SW China. *Acta Geol. Sin.* **2016**, *90*, 857–872.
29. Li, Y.; Allen, P.A.; Zhou, R.J.; Densmore, A.L.; Ellis, M.A. Mesozoic-Cenozoic Dynamics of Longmenshan Foreland Basin along the Eastern Margin of the Tibetan Plateau and its Coupled Relationship with Continent Collision. *Acta Geol. Sin.* **2006**, *80*, 1101–1109. [[CrossRef](#)]
30. Lin, L.B.; Chen, H.D.; Hu, X.Q.; Ji, X.T.; Jiang, P. Classification of tectonic sequence and basin evolution of the upper Triassic in the Sichuan basin. *J. Stratigr.* **2007**, *04*, 415–422. [[CrossRef](#)]
31. Li, Z.W.; Chen, H.D.; Liu, S.G.; Hou, M.C.; Deng, B. Differential uplift driven by thrusting and its lateral variation along the Longmenshan belt, western Sichuan, China: Evidence from fission track thermochronology. *Chin. J. Geol.* **2010**, *45*, 944–968. [[CrossRef](#)]
32. Chen, B. The sedimentary characteristics and formation mechanism of black shale in the Southern Longmenshan Foreland Basin in the Late Triassic. *Chengdu Univ. Technol. Collage Energy* **2019**, *15*, 80–90. [[CrossRef](#)]
33. Chen, H.D.; Liu, L.; Lin, L.B.; Wang, X.L.; Wang, Z.W.; Yu, Y.; Zeng, J.; Li, P.W. Depositional responses of Xujiahe Formation to the uplifting of Longmenshan during the Late Triassic, Western Sichuan Depression. *Oil Gas Geol.* **2021**, *2021*, 801–815. [[CrossRef](#)]
34. Deng, B.; He, Y.; Huang, J.Q.; Luo, Q.; Yang, R.J.; Yu, H.; Zhang, J.; Liu, S.G. Analogue modeling insights to foreland basin growth: A case study on the Longmenshan Thrust Belt in Western Sichuan Basin. *Oil Gas Geol.* **2021**, *42*, 401–415.
35. Xu, Z.Q.; Wang, Q.; Li, Z.H.; Li, H.Q.; Cai, Z.H.; Liang, F.H.; Dong, H.W.; Cao, H.; Chen, X.J. Indo-Asian Collision: Tectonic Transition from Compression to Strike Slip. *Acta. Geol. Sin.* **2016**, *90*, 1–23. [[CrossRef](#)]
36. Golonka, J. Late Triassic and Early Jurassic Palaeogeography of the world. *Palaeogeogr. Palaeoclim. Palaeoecol.* **2007**, *244*, 297–307. [[CrossRef](#)]
37. Ogg, J.G.; Ogg, G.M.; Gradstein, F.M. *A Concise Geologic Time Scale*; Elsevier: Amsterdam, The Netherlands, 2016; pp. 133–149.
38. Yu, Y.; Lin, L.B.; Zhai, C.B.; Chen, H.D.; Wang, Y.N.; Li, Y.H.; Deng, X.L. Impacts of lithologic characteristics and diagenesis on reservoir quality of the 4th member of the Upper Triassic Xujiahe Formation tight gas sandstones in the western Sichuan Basin, southwest China. *Mar. Pet. Geol.* **2019**, *107*, 1–19. [[CrossRef](#)]
39. Tan, C.; Yu, B.S.; Ruan, Z.; Hao, S.L.; Li, K.; Luo, Z.; Liu, R.D. High-Resolution Sequence Stratigraphy Research for Xujiahe Formation of the Upper Triassic Series in Sichuan Basin. *Geoscience* **2017**, *31*, 290–301. [[CrossRef](#)]
40. Liu, S.G.; Li, Z.W.; Sun, W.; Deng, B.; Huang, W. Basic geological features of superimposed basin and hydrocarbon accumulation in Sichuan basin, China. *Chin. J. Geol.* **2011**, *46*, 233–257.
41. Liu, S.G.; Deng, B.; Sun, W.; Zhong, Y.; Li, Z.W.; Li, J.X.; Jiang, L. Sichuan Basin: A superimposed basin formed under the main control of peripheral activities. *Chin. J. Geol.* **2018**, *53*, 308–326.
42. Xu, Y.Y. New fossil materials from the Upper Triassic Xujiahe Formation in the Sichuan Basin and their palaeoenvironmental significances. *Univ. Sci. Technol. China* **2020**, *1*, 124. [[CrossRef](#)]
43. Tian, N.; Wang, Y.D.; Philippe, M.; Li, Q.; Xie, X.P.; Jiang, Z.K. New record of fossil wood Xenoxylon from the Late Triassic in the Sichuan Basin, southern China and its paleoclimatic implications. *Palaeogeogr. Palaeoclim. Palaeoecol.* **2016**, *464*, 65–75. [[CrossRef](#)]
44. Zhou, N.; Wang, Y.D.; Li, L.Q.; Zhang, X.Q. Diversity variation and tempo-spatial distributions of the Dipteridaceae ferns in the Mesozoic of China. *Palaeoworld* **2016**, *25*, 263–286. [[CrossRef](#)]

45. Lu, N.; Wang, Y.D.; Popa, M.E.; Xie, X.P.; Li, L.Q.; Xi, S.N.; Xin, C.L.; Deng, C.T. Sedimentological and paleoecological aspects of the Norian-Rhaetian transition (Late Triassic) in the Xuanhan area of the Sichuan Basin, Southwest China. *Palaeoworld* **2019**, *28*, 334–345. [[CrossRef](#)]
46. Chen, C.Y.; Wang, Q.X.; Chen, D.F. Genesis of Siderite in Miocene Marine Shale in Kuohsing Area, Taiwan. *Acta Sedimentol. Sin.* **2021**, *40*, 1691–1701. [[CrossRef](#)]
47. Lu, Y.F.; Meng, W.B.; Feng, M.S.; Zhang, C.G.; Wang, J.; Wang, X.; Zhang, Y. Characteristics of the Middle Triassic Mung Beans Rock in the Mount Emei Area and their Implications for Sedimentary Environment. *Bull. Mineral. Petrol. Geochem.* **2020**, *39*, 626–636. [[CrossRef](#)]
48. McLennan, S.M.; Taylor, S.R. Sedimentary rocks and crustal evolution: Tectonic setting and secular trends. *J. Geol.* **1991**, *99*, 1–21. [[CrossRef](#)]
49. Bai, Y.Y.; Liu, Z.J.; Sun, P.C.; Rong, L.; Hu, X.F.; Zhao, H.Q.; Xu, Y.B. Rare earth and major element geochemistry of Eocene fine-grained sediments in oil shale- and coal-bearing layers of the Meihe Basin, Northeast China. *J. Asian Earth Sci.* **2015**, *97*, 8–101. [[CrossRef](#)]
50. Dai, S.F.; Graham, I.T.; Ward, C.R. A review of anomalous rare earth elements and yttrium in Coal. *Int. J. Coal Geol.* **2016**, *159*, 82–95. [[CrossRef](#)]
51. Shields, G.; Stille, P. Diagenetic constraints on the use of cerium anomalies as palaeoseawater redox proxies: An isotopic and REE study of Cambrian phosphorites. *Chem. Geol.* **2001**, *175*, 29–48. [[CrossRef](#)]
52. Cao, T.T.; Xu, S.H.; Wang, Y. Characteristics of rare earth elements in Lower Cambrian Qiongzhusi Formation in Northeastern Sichuan Basin and its geological implications: A case study of Yangba section, Nanjiang. *Petrol Geol. Exp.* **2018**, *40*, 716–723. [[CrossRef](#)]
53. Wang, Q.W.; Kan, Z.H.; Liu, X.H.; Liang, B.; Zhu, B. The Mesozoic Sporopollen Assemblage in the Sichuan Basin and Its Significance to Paleovegetation and Paleoclimate. *Acta Geol. Sichuan.* **2008**, *2*, 89–95.
54. Liu, Z.S.; Li, L.Q.; Wang, Y.D. Late Triassic Spore-Pollen assemblage from the Xujiahe Formation in Hechuan of Chongqing, China. *Acta Palaeontol. Sin.* **2015**, *54*, 279–304. [[CrossRef](#)]
55. Zhao, Z.Y.; Zhao, J.H.; Wang, H.J.; Liao, J.D.; Liu, C.M. Distribution characteristics and applications of trace elements in Junggar Basin. *Nat. Gas Explor. Develop.* **2007**, *30*, 30–33. [[CrossRef](#)]
56. Meng, Q.T.; Liu, Z.J.; Bruch, A.A.; Liu, R.; Hu, F. Palaeoclimatic evolution during Eocene and its influence on oil shale mineralization, Fushun basin, China. *Asian Earth Sci.* **2012**, *45*, 95–105. [[CrossRef](#)]
57. Cao, H.S.; Guo, W.; Shan, X.L.; Ma, L.; Sun, P.C. Paleolimnological environments and organic accumulation of the Nenjiang Formation in the Southeastern Songliao Basin, China. *Oil Shale* **2015**, *32*, 5–24. [[CrossRef](#)]
58. Wang, Z.; Wang, J.; Fu, X.; Zhan, W.; Armstrong-Altrin, J.S.; Yu, F.; Feng, X.L.; Song, C.Y.; Zeng, S.Q. Geochemistry of the Upper Triassic black mudstones in the Qiantang Basin, Tibet: Implications for paleoenvironment, provenance, and tectonic setting. *J. Asian Earth Sci.* **2018**, *160*, 118–135. [[CrossRef](#)]
59. Zheng, Y.W.; Fu, D.L.; Tian, B.; Duan, Z.Q.; Zhang, B.; Luo, J.N.; Wang, Z.X. The mineral composition and geochemical characteristics of rare earth elements of Salt Lake shale in Qianjiang Depression and its geological significance. *Mar. Orig. Petrol Geol.* **2021**, *26*, 150–158. [[CrossRef](#)]
60. Dymond, J.; Suess, E.; Lyle, M. Barium in deep-sea sediment: A geochemical proxy for paleo productivity. *Paleoceanography* **1992**, *7*, 163–181. [[CrossRef](#)]
61. Algeo, J.T.; Kuwahara, K.; Sano, H.; Bates, S.; Lyons, T.; Elswick, E.; Hinnov, L.; Ellwood, B.; Moser, J.; Maynard, J.B. Spatial variation in sediment fluxes, redox conditions, and productivity in the Permian-Triassic Panthalassic Ocean. *Paleogeogr. Paleoclim. Paleocol.* **2011**, *308*, 65–83. [[CrossRef](#)]
62. Dong, T.; Harris, N.B.; Ayranci, K. Relative sea-level cycles and organic matter accumulation in shales of the Middle and Upper Devonian Horn River Group, northeastern British Columbia, Canada: Insights into sediment flux, redox conditions, and bio productivity. *GSA Bull.* **2018**, *130*, 859–880. [[CrossRef](#)]
63. He, Q.; Gao, J.; Dong, T.; He, S.; Zhai, G.Y.; Zou, G.F. Elemental Geochemistry and Paleo-environmental Conditions of the Lower Cambrian Niutitang Shale in Western Hubei Province. *Acta Sedimentol. Sin.* **2021**, *39*, 686–703. [[CrossRef](#)]
64. Zhai, G.Y.; Li, J.; Jiao, Y.; Wang, Y.F.; Liu, G.H.; Xu, Q.; Wang, C.; Chen, R.; Guo, X.B. Applications of chemo stratigraphy in a characterization of shale gas Sedimentary Microfacies and predictions of sweet spots-taking the Cambrian black shales in Western Hubei as an example. *Mar. Pet. Geol.* **2019**, *109*, 547–560. [[CrossRef](#)]
65. Xu, J.; Pu, R.H.; Yang, L.; An, H. The Palaeosalinity Analysis of Carboniferous Mudstone, Tarim Basin. *Acta Sedimentol. Sin.* **2010**, *28*, 509–517. [[CrossRef](#)]
66. Fan, Y.H.; Qu, H.J.; Wang, H.; Yang, X.C.; Feng, Y.W. The application of trace elements analysis to identifying sedimentary media environment: A case study of Late Triassic strata in the middle part of Western Ordos Basin. *Geol. China* **2012**, *39*, 382–389. [[CrossRef](#)]
67. Stanistreet, I.G.; Boyle, J.F.; Stollhofen, H.; Deocampo, D.M.; Deino, A.; McHenry, L.J.; Toth, N.; Schick, K.; Njau, J.K. Palaeosalinity and palaeoclimatic geochemical proxies (elements Ti, Mg, Al) vary with Milankovitch cyclicity (1.3 to 2.0 Ma), OGCP cores, Palaeolake Olduvai, Tanzania. *Paleogeogr. Paleoclim. Paleocol.* **2020**, *546*, 109656. [[CrossRef](#)]
68. He, Y.Y.; Zhao, G.T.; Zhao, L.; Long, X.J.; Qi, Q.; Xu, C.L. Geochemistry Characteristics and Palaeo-Environment Significance of Qixia Formation in Chaobei Area. *Period. Ocean. Univ. China* **2014**, *44*, 79–88. [[CrossRef](#)]

69. Zhang, L.T. Geochemical characteristics and geological significance of organic-rich shale in Chongqing area. *China Univ. Geosci. Sch. Ocean. Sci.* **2019**, *2*, 33–52. [[CrossRef](#)]
70. Dai, C.C.; Ren, J.P.; Rao, Q.; Zhang, H.S. Paleosalinity of the Xujiahe Formation in Central Sichuan Basin and Its Geological Significance. *Geol. J. China Univ.* **2018**, *24*, 390–400. [[CrossRef](#)]
71. Lai, W. Geochemical characteristics of Xujiahe Formation mudstones in the northeast Sichuan and their geological significance. *China Univ. Geosci.* **2020**, *8*, 70. [[CrossRef](#)]
72. McKirdy, D.M.; Hall, P.A.; Nedin, C.; Halverson, G.P.; Michaelsen, B.H.; Jago, J.B.; Gehling, J.G.; Jenkins, R.J.F. Paleoredox status and thermal alteration of the lower Cambrian (Series 2) Emu Bay Shale Lagerstätte, South Australia. *Aust. J. Earth Sci.* **2011**, *58*, 259–272. [[CrossRef](#)]
73. Dill, H. Metallogenies of early Paleozoic graptolite shales from the Graefenthal Horst (Northern Bavaria, Federal Republic of Germany). *Econ. Geol.* **1986**, *81*, 889–903. [[CrossRef](#)]
74. Tong, L.; He, Y.B.; Li, H. Sedimentary Environment of Late Ordovician Carbonates in the Fuping Area, Shaanxi Province. *Bull. Mineral. Petrol. Geochem.* **2019**, *38*, 748–758. [[CrossRef](#)]
75. Algeo, T.J.; Tribouillard, N. Environmental analysis of palaeoceanographic systems based on molybdenum-uranium covariation. *Chem. Geol.* **2009**, *268*, 211–225. [[CrossRef](#)]
76. Li, Y.F.; Shao, D.Y.; Lv, H.G.; Zhang, X.L.; Zhang, Y.W. A relationship between elemental geochemical characteristics and organic matter enrichment in marine shale of Wufeng Formation-Longmaxi Formation, Sichuan Basin. *Acta Pet. Sin.* **2015**, *36*, 1470–1483. [[CrossRef](#)]
77. Wang, W.; Zhou, M.F.; Yan, D.P.; Li, J.W. Depositional age, provenance, and tectonic setting of the Neoproterozoic Sibao Group, Southeastern Yangtze Block, South China. *Precambrian Res.* **2012**, *192–195*, 107–124. [[CrossRef](#)]
78. Hou, Q.; Mou, C.L.; Wang, Q.Y.; Tan, Z.Y.; Ge, X.Y.; Wang, X.P. Geochemistry of sandstones from the Silurian Hanxia formation, North Qilian Belt, China: Implication for provenance, weathering and tectonic setting. *Geochem. Int.* **2018**, *56*, 362–377. [[CrossRef](#)]
79. Li, J.; Tian, J.C.; Zhang, X.; Liang, Q.S.; Peng, M.H. Geochemical characteristics and the constraints on paleoenvironment, provenance, and tectonic setting of Precambrian Xifangshan Formation in the northwestern Tarim Basin, NW China. *J. Petrol. Sci. Eng.* **2022**, *208*, 109553. [[CrossRef](#)]
80. Awasthi, N. Provenance and paleo-weathering of Tertiary accretionary prism-forearc sedimentary deposits of the Andaman Archipelago, India. *J. Asian Earth Sci.* **2017**, *150*, 45–62. [[CrossRef](#)]
81. Oghenekome, M.E.; Chatterjee, T.K.; van Bever Donker, J.M.; Hammond, N.Q. Geochemistry and weathering history of the Balfour sandstone formation, Karoo basin, South Africa: Insight to provenance and tectonic setting. *J. Afr. Earth Sci.* **2018**, *147*, 623–632. [[CrossRef](#)]
82. Sahariah, N.; Bhattacharyya, P. Geochemical characteristics of the Tura Formation in parts of the Upper Assam Basin: An implication on provenance, tectonic setting and source-Area Weathering. *J. Appl. Geochem.* **2019**, *21*, 1–14.
83. Cullers, R.L.; Podkovyrov, V.N. Geochemistry of the Mesoproterozoic Lakhanda shales in Southeastern Yakutia, Russia: Implications for mineralogical and provenance control, and recycling. *Precambrian Res.* **2000**, *104*, 77–93. [[CrossRef](#)]
84. Cullers, R.L.; Podkovyrov, V.N. The source and origin of terrigenous sedimentary rocks in the Mesoproterozoic Ui group, Southeastern Russia. *Precambrian Res.* **2002**, *117*, 157–183. [[CrossRef](#)]
85. Nesbitt, H.W.; Young, G.M. Early Proterozoic climates and plate motions inferred from major element chemistry of lutites. *Nature* **1982**, *299*, 715–717. [[CrossRef](#)]
86. Cox, R.; Lowe, D.R.; Cullers, R.L. The influence of sediment recycling and basement composition on evolution of mudrock chemistry in the southwestern United States. *Geochim. Et Cosmochim. Acta* **1995**, *59*, 2919–2940. [[CrossRef](#)]
87. Wu, F.Z.; Liu, D.N.; Zhao, F.H.; Zou, Y.; Xie, A.K.; Li, J.S. Sedimentary conditions and geotectonic setting implicated from the geochemistry of major and trace elements in pelite of the Sugetbrak Formation in Northwestern of Tarim Basin, Xinjiang, China. *Bull. Mineral. Petrol. Geochem.* **2021**, *40*, 478–490. [[CrossRef](#)]
88. McLennan, S.M.; Hemming, S.; McDaniel, D.K.; Hanson, G.N. Geochemical Approaches to Sedimentation, Provenance, and Tectonics. In *Processes Controlling the Composition of Clastic Sediments*; Johnson, M.J., Basu, A., Eds.; Geological Society of America: Boulder, CO, USA, 1993; Volume 284, pp. 21–40. [[CrossRef](#)]
89. Fedo, C.M.; Nesbitt, H.W.; Young, G.M. Unraveling the Effects of potassium metasomatism in Sedimentary Rocks and Paleosols, with implications for paleo weathering conditions and provenance. *Geology* **1995**, *23*, 921–924. [[CrossRef](#)]
90. Nesbitt, H.W.; Young, G.M. Prediction of some weathering trends of plutonic and volcanic rocks based on thermodynamic and kinetic considerations. *Geochim. Et Cosmochim. Acta* **1984**, *48*, 1523–1534. [[CrossRef](#)]
91. Young, G.M.; Nesbitt, H.W. Paleoclimatology and provenance of the Glaciogenic Gowganda Formation (Paleoproterozoic), Ontario, Canada: A chemostratigraphic approach. *GSA Bull.* **1999**, *111*, 264–274. [[CrossRef](#)]

92. Mou, C.L.; Ge, X.Y.; Yu, Q.; Men, X.; Liu, W.; He, J.L.; Liang, W. Palaeoclimatology and provenance of black shales from Wufeng-Longmaxi Formations in southwestern Sichuan Province: From geochemical records of Well Xindi-2. *J. Palaeogeogr. Chin. Ed.* **2019**, *21*, 835–854. [[CrossRef](#)]
93. Xu, X.T.; Shao, L.Y. Limiting factors in utilization of chemical index of alteration of mudstones to quantify the degree of weathering in provenance. *J. Palaeogeogr. Chin. Ed.* **2018**, *20*, 515–522. [[CrossRef](#)]

**Disclaimer/Publisher’s Note:** The statements, opinions and data contained in all publications are solely those of the individual author(s) and contributor(s) and not of MDPI and/or the editor(s). MDPI and/or the editor(s) disclaim responsibility for any injury to people or property resulting from any ideas, methods, instructions or products referred to in the content.